Femtosecond Laser Fabrication of Directional Couplers and Mach-Zehnder Interferometers

by
Yu Gu
B.S. Engineering Physics
Cornell University, Ithaca, NY 2005.

SUBMITTED TO THE DEPARTMENT OF ELECTRICAL ENGINEERING AND COMPUTER SCIENCE IN PARTIAL FULFILLMENT OF THE REQUIREMENTS FOR THE DEGREE OF

MASTER OF SCIENCE IN ELECTRICAL ENGINEERING AND COMPUTER SCIENCE
AT THE
MASSACHUSETTS INSTITUTE OF TECHNOLOGY

SEPTEMBER 2007

Signature of Author:

_____

Yu Gu
Department of Electrical Engineering and Computer Science
August 31,2007

Certified by:

_____

James G. Fujimoto
Professor of Electrical Engineering and Computer Science
Thesis Supervisor

Accepted by:

_____

Chairman, Department Committee on Graduate Students

Femtosecond Laser Fabrication of Directional Couplers and Mach-Zehnder Interferometers

by

Yu Gu

Submitted to the Department of Electrical Engineering and Computer Science
on August 31, 2007 in Partial Fulfillment of the Requirements for the Degree of
Master of Science in Electrical Engineering and Computer Science

Abstract

The use of femtosecond lasers for photonic device fabrication in glass has become an active area of research in recent years. Since the first demonstration of laser modification of refractive index in glass, a variety of devices such as couplers, interferometers, gratings, 3D structures, active waveguides, and void structures have been successfully demonstrated. In contrast to conventional semiconductor-based fabrication processes, the femtosecond laser fabrication process utilizes a single step, enabling rapid prototyping of a variety of devices, including three-dimensional structures.

In order to make progress toward the building of more complex photonic structures, it is important to fabricate reliable couplers and Mach-Zehnder interferometers. To enable telecommunications applications, it is useful to demonstrate their functionality around 1550 nm. We demonstrate the femtosecond laser fabrication of symmetric directional couplers and unbalanced Mach-Zehnder interferometers and the measurement of their wavelength characteristics. We demonstrate an in-depth characterization of the spectral characteristics of symmetric directional couplers and show that they can be tailored by controlling the physical parameters of the device. A wavelength-independent 3dB directional coupler is designed for the wavelength range of 1500 to 1600 nm. We demonstrate high extinction Mach-Zehnder devices over the same wavelength range. The spectral data from a series of unbalanced Mach-Zehnders is used to find the waveguide propagation constant. In addition, the change in spectral behavior of Mach-Zehnders device is used to estimate the dependence of waveguide propagation constant on writing speed. The ability to fabricate couplers and Mach-Zehnder devices with good repeatability and flexibility is an important step toward the design of complex femtosecond laser written integrated devices

Thesis Supervisor: James G. Fujimoto
Title: Professor of Electrical Engineering and Computer Science

Acknowledgements

I would like to thank my research advisor and thesis supervisor, Professor James Fujimoto. Without his guidance, leadership, and resources, this work would not have been possible. I would like to thank my collaborator Dr. Jung-Ho Jung, for my training, and for his suggestions and technical support. I would also like to thank other members of my group, including Shu-Wei Huang, Umit Demirbas, Jonathan Liu, Vivek Srinivasan, Desmond Adler, Dr. Yu Chen, Dr. Iwona Gorczynska as well as previous group members Aaron Aguirre and Dr. Robert Huber. I would also like to thank especially Dr. Andrew Kowalevicz for his long-distance support, as well as professors Franz Kartner, Alphan Sennaroglu and Helder Crespo.

I would like to acknowledge Cornell University, especially the department of Applied and Engineering Physics, for equipping me with the tools necessary to begin my graduate career. I would like to acknowledge the financial support from Air Force Office of Scientific Research grants FA9550-040-1-0046 and FA9550-040-1-0011 and National Science Foundation grant BES-0522845.

I am very grateful to my parents, both of whom were PhD students once, for the many night phone calls about how to perform research. I would like to thank Professor Leslie Kolodziejski for her support both as a mentor and as a friend. Most importantly, I would like to thank the people who kept me sane day after day, my friends Shuodan Chen, Michelle Sander, Nicole Dilello, Elizabeth Bass, and many others. I am grateful for having had the opportunity and resources to produce something of scientific value, and hope that I can continue on to more.

TABLE OF CONTENTS

CHAPTER 1: INTRODUCTION

1.1 Background of Femtosecond Laser Fabrication

1.1.1 Background

The use of femtosecond lasers for photonic waveguide fabrication in glass has become an active area of research in recent years. Using a tightly focused femtosecond laser beam, a region of modified index results from energy deposited through multi-photon absorption. This is illustrated in Fig 1.

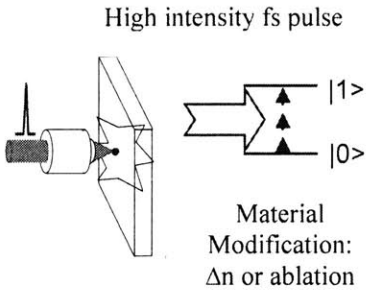

Fig 1. Concept of focusing a high intensity femtosecond pulse to generate index modification in glass

The first demonstration for modifying refractive index in glass using femtosecond laser irradiation was reported in 1996 [1] . By focusing 810 nm laser light through a microscope objective, the authors successfully wrote transparent, but visible, round-elliptical damage lines inside high-silica, borate, soda lime silicate, and fluorozirconate (ZBLAN) bulk glasses. Since then, various photonic devices have been fabricated using femtosecond nonlinear material processing and it has become a powerful and versatile technique. In contrast to conventional semiconductor-based fabrication processes, the femtosecond writing process utilizes a single step fabrication, enabling rapid prototyping of a variety of devices including three-dimensional structures. The capability of writing three-dimensional structures has the potential for enabling high-density integrated photonic circuits, providing enhanced functionality not possible in planar geometries.

A variety of devices in glasses such as couplers, interferometers, gratings, 3D structures, active waveguides and void structures have been successfully demonstrated [2-7]. Since material interaction is mediated by nonlinear effects, there is strong dependence of waveguide properties such as index of refraction, mode size, and loss, on writing parameters such as power and speed. One aspect which is important to understand is the mechanism of index modification and how waveguide properties vary with different exposure parameters. It has been suggested that index modification is a result of local densification of the glass[8], however the mechanism of index modification is nonlinear with respect to exposure power and is yet to be completely understood [8]. Loss, mode number and mode shape depend upon exposure parameters such as power and writing speed [9, 10]. Eaton et al. studied heat accumulation effects in femtosecond laser writing of waveguides, demonstrating that high-repetition rate femtosecond lasers produce heat accumulation effects which are desirable for rapid prototyping of low-loss optical waveguides [11]. In that study, an amplified Yb-fiber laser with 375 fs pulse length at 1045 nm was shown to produce cumulative heating effects while writing straight waveguides at repetition rates above around 200 kHz [11]. Waveguides produced in this regime had lower loss (as little as 0.2dB/cm in Schott AF45 glass) and more symmetric cross-section profiles than with lower-repetition laser systems. Cumulative heating also enables fabrication to be performed at speeds on the order of 10 mm/s [3], three orders of magnitude higher than the fabrication speeds of lower repetition rate laser systems. Another recent study supports the theory of cumulative heating as the mechanism of energy deposition [44]. Using variable repetition rates and bursts of laser pulses, it was shown that the diameter of waveguides grow with increasing burst number at all repetition rates, but cumulative heating has an onset threshold of 1.5 MHz for a Ti:sapphire system.

In order to fabricate and characterize the devices in the following studies, it is necessary to understand the nature of photonic devices which have been previously demonstrated and their possible applications. It is also necessary to review the characterization of index change and how to predict the size and shape of the waveguide modes.

1.1.2 Photonic devices

Alongside characterization of basic waveguide properties, a range of passive photonic devices have been fabricated using femtosecond exposure [2-6]. In addition, femtosecond writing has

been used to produce active optical waveguides in doped glasses [12, 13], and more complex devices (Mach-Zehnder interferometers) are being written in active materials [14].

Photonic devices such as splitters and coupled mode devices are the building blocks of more complex devices which are of interest in many applications including telecommunications and sensing. X-couplers with 1-1 and 16-1 power splitting ratios were fabricated by our group at MIT using a novel MPC Ti:sapphire oscillator [15]. 1x2 optical splitters with around 6.55 dB insertion loss which can be cascaded into 1xn splitters have also been demonstrated by other groups [16]. A multi-scan technique in which part of the splitter is written a second time was developed to reduce insertion loss and polarization dependent loss of the Y junctions [16]. Cubic lattices of straight waveguides have been shown to demonstrate discrete diffraction behavior through evanescent coupling [17]. These devices have output intensity patterns which agree well with theoretical prediction, demonstrating favorable waveguide fabrication. Furthermore, excitation of a single input waveguide results in splitting of power at the end surface, effectively producing a 1-to-n splitter.

Since femtosecond laser fabrication enables direct-writing of structures at different depths within a single substrate without causing collateral damage effects, it has the advantage of being able to produce three-dimensional structures. It has been demonstrated that a single substrate can contain layered, independent devices such as [1xn] splitters[18]. Furthermore, splitters, couplers, and other photonic devices are not limited to two dimensional geometries. Using fabrication in three-dimensions, a [1x3] splitter has been realized[19]. It is possible to fabricate devices in novel three-dimensional geometries, such as the [1x4] splitter shown below in Fig. 2 [20]. Note that this device is created by cascading two [1x2] x-couplers.

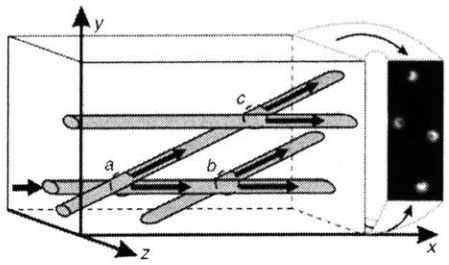

Fig. 2 from ref [20] Schematic of 1x4 coupler created by combining two 1x2 couplers. The diagram on the right shows the experimental near-field output at 1550nm.

An example of a more complex three-dimensional device is the symmetric [3x3] directional coupler [21]. The [3x3] coupler has a triangular geometry shown in Fig. 4, and the coupling ratios of each output closely agree with theory. By utilizing the third dimension, it is possible to fabricate devices with novel geometries. Higher device density is achievable, and this new class of devices promises increased functionality and greater compactness.

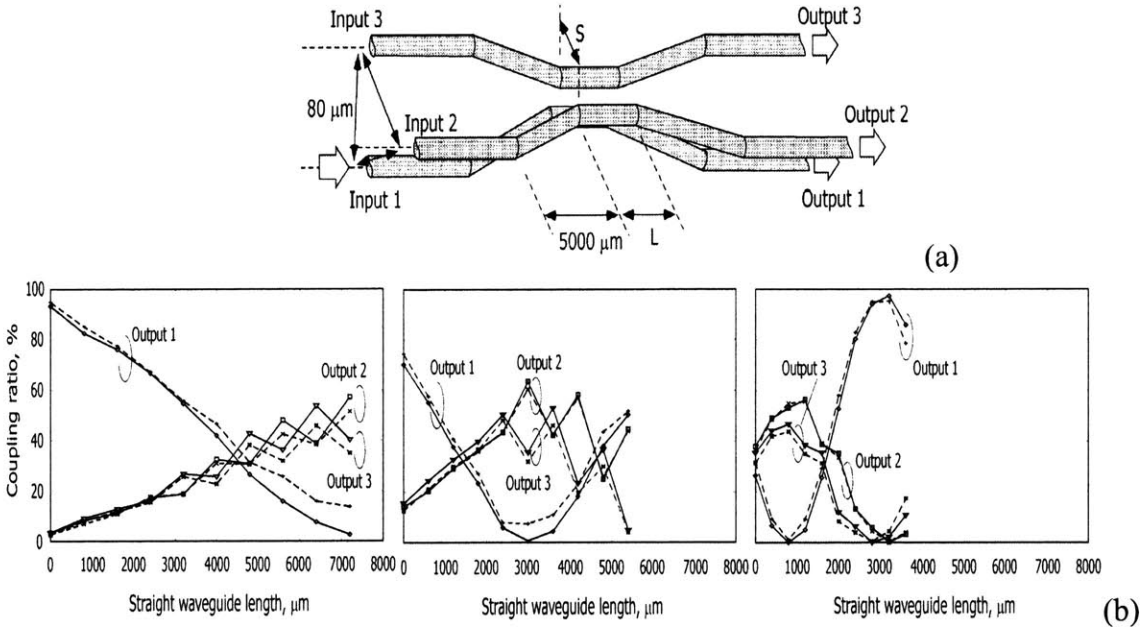

Fig. 3 from ref [21] (a) Schematic of the 3x3 directional coupler. (b) Output characteristics of the 3x3 coupler with three different interaction separations, 25um, 20um, and 15um.

The realization of splitters and coupled mode devices enabled recent advances in the femtosecond laser fabrication of interferometric devices. An earlier demonstration of a mach-zehnder interferometer consisted of two X-couplers placed back-to-back[3]. Mach-Zehnder Interferometers have applications in sensing changes in external parameters in one arm and are also used in telecommunication networks to separate or combine signals. The ability to fabricate such devices with good repeatability requires being able to control the path length difference between the two arms with a high level of precision. It is also important to understand how to tune MZI devices to achieve the desired wavelength response. Recently, it has been shown that devices such as interferometers can be tuned after initial fabrication to achieve desirable characteristics, a process called "trimming"[22]. "Trimming" is the process of tuning existing device characteristics through additional laser exposure. Assuming that index of refraction can

be modified cumulatively, additional laser exposure creates longer optical paths by making additional changes to the index. Trimming can be used to improve the contrast ratio of Mach-Zehnder devices by optimizing couplers for 3dB operation through the increase of the interaction optical path length. Trimming can also be used to change the waveguide's cross-section, giving the ability to correct polarization-dependent behavior [22].

1.1.3 Applications

Femtosecond laser fabricated waveguide devices can be used in various telecommunications and sensing applications. For example, both straight waveguides and interferometers can be used as sensor devices. An optical vibrational sensor fabricated using femtosecond laser oscillator consisting of a straight waveguide written cross three pieces of glass, with the central piece mounted on a suspended beam, has been shown to have a linear response to external vibrations over the frequency range 20 Hz to 2 kHz [23].

The femtosecond laser fabrication of waveguide devices has been demonstrated in active materials, enabling the application of femtosecond writing for active device production. In 2003, Osellame et al demonstrated a novel technique for waveguide fabrication based on astigmatic shaping of the writing beam [25]. By reducing the beam dimension along the transverse direction and offsetting the focusing positions of the two beam waists, it was possible to obtain symmetric profiles, thereby overcoming the limitation of low repetition rate laser writing systems. Using this technique, single mode waveguides were written in active Er-Yb doped glass substrates. 9 mm long waveguides demonstrated a gain of 1.4 dB. Using longer waveguides to create higher gain was limited by the short absorption lengths resulting from the high Yb concentration. The use of substrates with reduced doping or detuned pump diodes should enable substantially higher gains, allowing for the production of waveguide amplifiers and lasers. This was an important demonstration for the production of active devices using femtosecond laser writing. Increase of writing speed, which was limited to 20 um/s by the low repetition rate, could be achieved with higher repetition rates, opening the possibility of industrial production. Fig. 4 shows the measured absorption and gain values for the 9 mm

waveguide in Er-Yb doped glass. The curves are theoretical fits calculated with known absorption and emission cross sections.

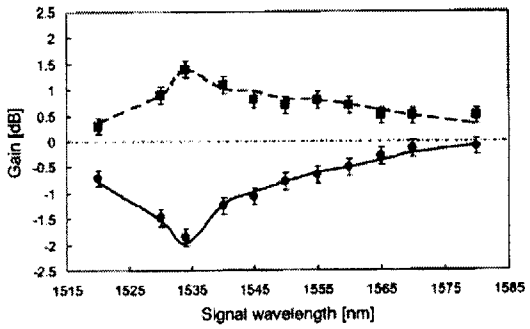

Fig 4. from ref [25] Measured absooption and gain for a 9 mm long femtosecond written waveguide in Er-Yb doped glass.

Soon after the demonstration of optical gain in a femtosecond laser written waveguide, a single mode waveguide laser emitting at 1.5 um was fabricated in Er-Yb doped phosphate glass [26] This device had more than 50 mW of output power and had 21% slope efficiency. Passive mode-locking in a femtosecond written waveguide in Er-Yb doped phosphase glass soon followed [27]. Passive mode locking was obtained using a specially designed fiber-pigtailed carbon nanotube absorber incorporated into a monolithic laser structure. The waveguide laser was operated in a ring cavity configuration, while pump with two 976 nm laser diodes providing 480 mW of incident power. Lasing threshold is at 450 mW of pump power, and self-starting mode-locking is observed immediately above the laser threshold. The pulse width, as measured by autocorrelation, is 2.72 ps, and the spectrum has FWHM of 1.6 nm centered at 1535 nm. The repetition rate of the cavity was 16.74 MHZ, although it could be changed by altering the cavity configuration. The laser efficiency was low (output power was about 0.1 mW) due to relatively high insertion losses inside the cavity. This was an important step toward the application of femtosecond laser waveguide writing to the manufacturing of active devices. Creating light sources is important for the building of complex photonic devices. By reducing intra-cavity losses and optimizing dispersion, it may be possible to use a larger portion of the Er gain bandwidth and achieve femtosecond laser operation.

Another application of femtosecond laser waveguide fabrication is the creation of micro-channels. Micro-channels created in glass substrates have applications in micro-photonics, micro-electronics, and micro-fluidics. Material can be removed from a substrate either by direct

ablation [28,29] or chemical etching following laser exposure [24-27]. At high NA focusing, studies suggest that energy from the laser pulse is absorbed by the material through nonlinear absorption or linear absorption by plasma, resulting in bulk damage [28]. A study done on morphology of femtosecond laser-induced structural changes suggests that voids appearing in the material at higher laser energies are from hot electrons and ions explosively expanding into surrounding regions [29]. Multiple-pulse sequences from a 1kHz repetition rate Ti:sapphire laser can produce channels as deep as 400um in amorphous silica with reduced fracturing levels compared to single pulses [36], while amplified Ti:sapphire, Cr:LiSAF, and Nd:YAG systems can drill holes as deep as 1mm in soda-lime glass [6]. To demonstrate application to microfluidic structures, frequency-doubled Ti:sapphire lasers have been used to fabricate channels, reservoirs, and through-holes on tenths of a micrometer scale in Pyrex glass and various polymers (PMMA, Pi, Kapton), providing good-quality finishing for passive fluid transport [30]. Three-dimensional interconnected micro-channel networks consisting of 10um diameter channels with arbitrary connecting angles have been fabricated inside silica glass using the two-step process of amplified Ti:sapphire laser exposure followed by etching with HF based etchants[32]. Resulting channels are optically transparent, enabling optical characterization techniques (transmission, photoluminescence, and Raman scattering for instance) to be performed with relative ease.

1.2 Mechanism of Index Modification

The mechanism of index modification is based on plasma generation from multiphoton absorption. The details of index modification remains a topic of research. The multiple-pass cavity laser source used in this study is designed to create waveguides in a cumulative heating regime. Cumulative heating occurs in high repetition rate laser writing systems where the interval between laser pulses is shorter than the time required for the absorbed energy to diffuse out of the focal volume. This was modeled numerically in Fig 5 [11].

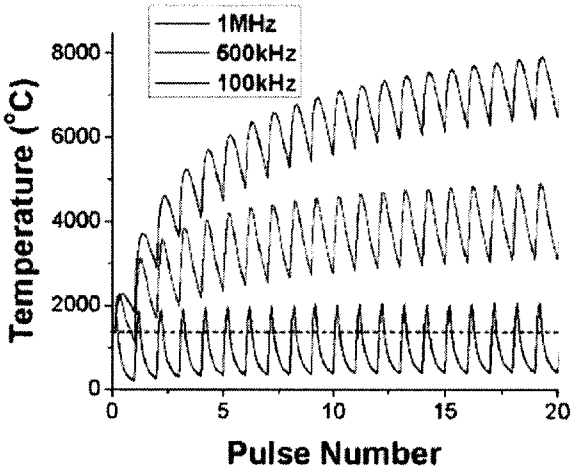

Fig. 5 from ref [11]. Finite-difference model of glass temperature versus exposure at 2 um radial distance from center of the laser beam. Cumulative heating results when the interval between laser pulses is shorter than the time required for the absorbed laser energy to diffuse out of the focal volume.

For the system discussed in this particular study, the cumulative heating effect was predicted to occur for lasers with repetition rates of 200 kHz and above. At 100 kHz, the sample temperature recovers fully to room temperature, so the melt-diffusion cycle occurs once per laser pulse with no cumulative effects. The melt radius of the waveguides as a function of net fluence was also calculated and agrees well with the melt radius measured from experimental waveguides. Waveguides produced with above 200 kHz repetition rates had lower loss (as little as 0.2dB/cm in Schott AF45 glass) and more symmetric cross-section profiles than with lower-repetition laser systems. Cumulative heating also enables fabrication to be performed at speeds on the order of 10 mm/s [3], three orders of magnitude higher than the fabrication speeds of lower repetition rate laser systems.

1.3 Solutions for waveguide modes

In order to understand the behavior of modes in femtosecond laser written waveguides, it is important to review theoretical solutions of modes in single-mode waveguides. The mode shape characteristics of a propagating guided wave are dependent on the shape and depth of the index profile. If the femtosecond laser written waveguide is modeled as a step-index circular waveguide, mode shapes and propagation characteristics can be modeled by solving the wave equation in cylindrical coordinates. Once modes are established, one can understand other important properties such as mode-cutoff conditions, numerical aperture, and normalized frequency.

The homogeneous wave equations in cylindrical coordinates is derived from the general wave equation:

$$\nabla^2 E - \mu\varepsilon \frac{\partial^2 E}{\partial t^2} = 0 \tag{1}$$

Since the z component of the field is the only component which does not couple to other components, the wave equation is derived in terms of the z component of the E field.

$$\frac{1}{r}\frac{\partial}{\partial r}\left(r\frac{\partial E_z}{\partial r}\right) + \frac{1}{r^2}\frac{\partial^2 E_z}{\partial \phi^2} + \frac{\partial^2 E_z}{\partial z^2} + k_0^2 n^2 E_z = 0 \tag{2}$$

This equation is solved through separation of variables, in which the z component of the E field is assumed to be a multiple of radial, angular, and propagation functions. The z-dependence is assumed to contain a phase term so $Z(z) = e^{-j\beta z}$. The standard separation of variables technique leads to a relatively simple solution for the angular dependence: $\Phi(\phi) = Ae^{-j\nu\phi}$. The equations for the radial dependence R(r) results from inserting the Z and Φ solutions back into the original wave equation. Thus we obtain:

$$r^2\frac{\partial^2 R}{\partial r^2} + r\frac{\partial R}{\partial r} + r^2(k_0^2 n^2 - \beta^2 - \frac{\nu^2}{r^2})R = 0 \tag{3}$$

The solutions for the radial dependence are Bessel functions. When the separation constant ν is an integer, the Bessel function solutions yield the dispersion relation:

$$k^2 = k_0^2 n^2 - \beta^2$$

(4)

To solve for the value of the propagation constant one must require boundary conditions to be consistent. This involves solving E and H field boundary conditions in both the radial and tangential cases. The tangential components of the E and H fields must both be continuous. The solutions are solved while assuming the field is confined and oscillatory inside the core or raised index region, and evanescent in the region outside the core. The equations lead to a 4x4 matrix which can be difficult to solve. For specific cases, however, the number of boundary value equations can be reduced. For purely transverse electric and transverse magnetic modes, for instance, the equations can be simplified. For the first TE mode, which is rotationally invariant, the separation constant v is set to 0, and the boundary condition equation is

$$\frac{J_1(ka)}{kJ_0} - \mu\varepsilon\frac{K_1(\gamma a)}{\gamma K_0(\gamma a)} = 0 \tag{5}$$

where J and K represent Bessel functions of the first and second kind, respectively. The two sides of the equation can be plotted in the same graph, and the intersection represents a solution for the transverse wavevector k, which can then be solved for the propagation constant. Mode cutoff conditions are determined by the roots of the appropriate Bessel functions. Fig 6 from ref 9 represents the graphical solution of the eigenvalue equation for a waveguide with core index 1.5 and cladding of 1.45 at wavelength 1.3 um. The arguments are plotted against the transverse propagation constant k. There is a non-zero solution for a mode whenever the curves intersect.

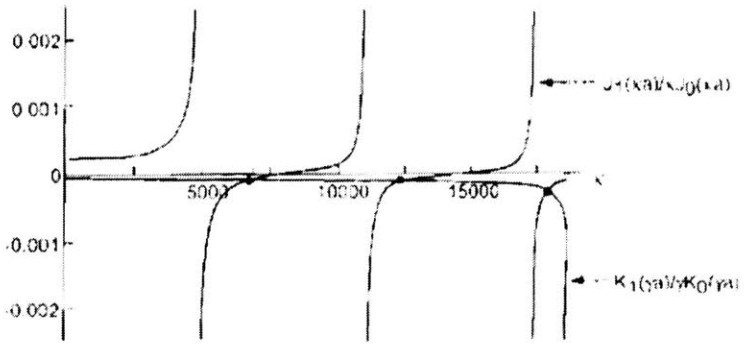

Fig 6 from ref [39] eigenvalue equations plotted against propagation constant k for waveguide with core index 1.5, cladding index 1.45 at 1.3 um wavelength.

Fig 7 from ref[39] shows the first three J Bessel functions. Cutoff conditions for the first few TE and LP (linearly polarized) modes are shown at the roots of the functions.

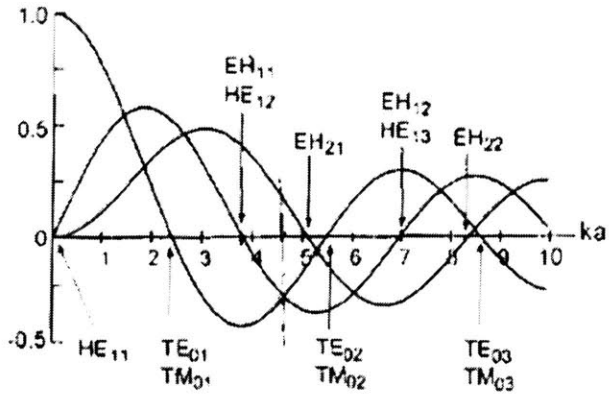

Fig 7 from ref [39] First three J_v Bessel functions. The roots represent mode cutoff conditions.

Notice that for the waveguides fabricated in this thesis, it is difficult to perform mode shape and propagation constant, since the exact index difference is not well-known. However, single-mode operation was confirmed by observing the output mode intensity profile.

1.4 Waveguide Characterization

Since it is important to understand the waveguide's index properties, various studies have been performed to characterize the index profiles of straight waveguides and the magnitude of index change. Laser pulse-induced refractive index change has been reconstructed from near-field mode profile data by imaging the end of the waveguide onto a CCD array, and calculating index from the intensity distribution by inverting the scalar-wave equation [31]:

$$n(x,y) \approx N_{eff} - \frac{\nabla^2 \sqrt{I(x,y)}}{2n_s k_o^2 \sqrt{I(x,y)}}.$$

This technique, however, requires very accurate mode-profile data which is limited by the quality of imaging onto the CCD array. For waveguides written with a 1 KHz Ti:sapphire laser in Nd-doped silicate glass, the change in refractive index was measured to be approximately $2\text{x}10^{-4}$ [41]. Refractive near-filed profilometer (RNF) has been used to examine cross-sectional

areas of waveguides produced with a 238 KHz Ti:sapphire laser, showing an elliptical shape which was dependent on writing geometry and a maximum index modification of around $3x10^{-3}$ [11]. Refractive index profilometry has also shown that waveguides written with low-repetition-rate lasers can have complex index profiles[19]. Fig. 1 shows the refractive index profile of a waveguide written in amorphous silica using a 300 fs Ti:sapphire laser at 2 MHz repetition rate measured using refractive index profilometry showing index change of up to $5x10^{-3}$ [19].

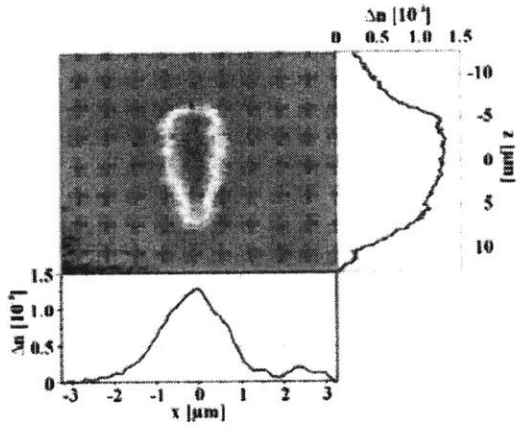

Fig.8. from ref [32] waveguide index profile of a waveguide written using a low repetition rate laser obtained using refractive index profilometry. The waveguide is shown to have an elliptical shape with refractive indices thare are dependent on writing conditions.

A less commonly used technique for measuring the index modification in femtosecond laser written waveguides is called optical low-coherence reflectometer (OLCR) [42]. OLCR is essentially a phase-measurement system based on a dual-channel Michelson interferometer with two independent channels of orthogonally polarized modes of a birefringent fiber. Light in the two channels is split into reference and sample paths, then the back-reflected signal from the sample and the reference signal are mixed to form an interference signal. Hilbert transform techniques are used on the interference signal to find the phase different between the sample and reference signals. This technique yields differential phase sensitivities of up to 0.01 radians. Using this technique, refractive index profiles of femtosecond laser written structures can be measured with 1-10 um of depth resolution.

Ultra-high resolution (20nm) index of refraction profiles of femtosecond laser fabricated structures measured using selective chemical etching and atomic force microscopy has also been demonstrated [43]. Since the process of index modification is highly nonlinear and some index

change features are as small as 50 nm, which cannot be measured with standard optically based index profiling techniques, the authors use chemical etching with 1% hydrofluoric acid followed by contact mode AFM. Fig. 9 shows the inverted image of the AFM topography profile of a femtosecond laser written waveguide.

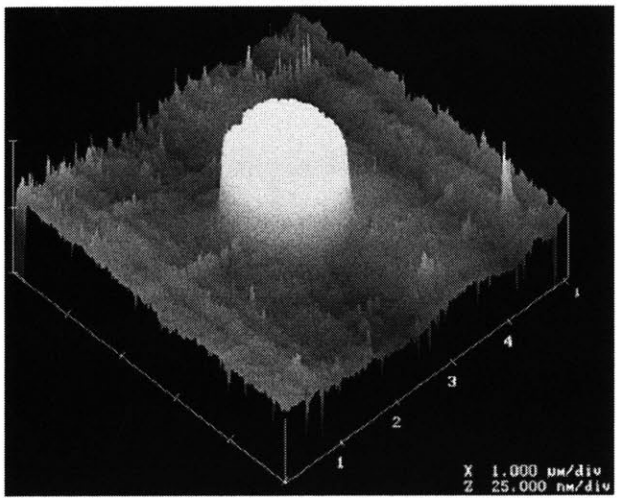

Fig 9 from ref [43] Inverted cros-sectional AFM image of a chemically etched waveguide written using a 250 kHZ Ti:Sapphire laser at 175 mW average power. The scan speed was 100 um/s. The image shows the size of the flatted-topped region as 1.7 um.

The lateral resolution of the image, as determined by the sharpness of the probe tips, is estimated to be between 15 and 20nm. The authors claim that the rate of etching of the waveguide is linearly dependent on the absolute index of refraction and therefore the absolute index profile is represented in the figure shown. The sharp index transition at the edges and the immediate transition to a flat-topped index profile is suggestive of nonlinear material index modification. A comparison of the index profile obtained using this technique and from microreflectivity measurements shows a first-order agreement, although microreflectivity gives an index profile with limited resolution. If valid, the method of chemical etching and AFM can be a straightforward technique that can measure absolute index of refraction changes of up to 0.01. However, this is not yet a universally accepted technique and refractive index profilometry remains the dominant index profiling technique for groups working on the characterization of femtosecond laser written waveguides.

In addition, waveguides have been imaged using Optical Coherence Tomography (OCT), which provides very accurate measurements of small index changes since it uses low coherence interferometry to generate cross-sectional images of backscattered or back-reflected light with high resolution and sensitivity. OCT imaging of cross-sectional areas of waveguides fabricated using a high-power 4MHz Ti:sapphire oscillator yielded refractive index changes as high as $9x10^{-3}$[15]. OCT has a high sensitivity to reflection of 10^{-10} and has axial and transverse resolutions of 1um and 3um. Fig. 10 shows the (a) schematic of the OCT measurement, (b) waveguide cross-section (c) OCT image and (d) recovered index profile of a waveguide from ref [15]. The top and bottom portions of the waveguide are clearly resolved.

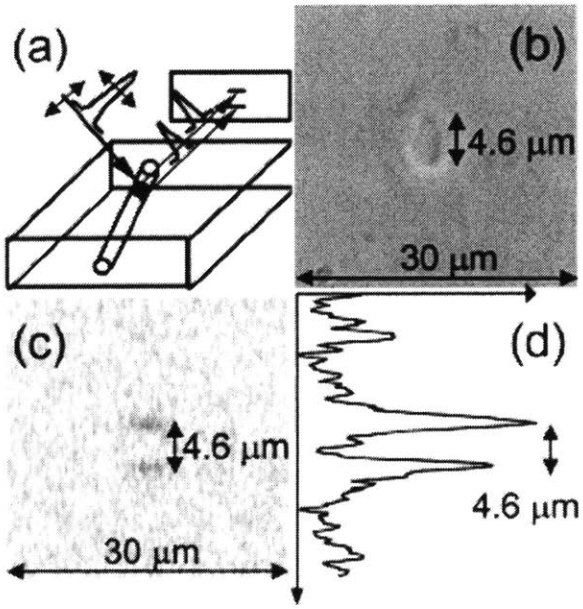

Fig 10. from ref [15]. (a) Schematic representation of OCT (b) and (c) show the microscope cross-sectional view and OCT image of a single-mode waveguide. (d) shows the recovered index profile.

OCT is capable of resolving small changes in index of femtosecond laser produced structures because of its high phase sensitivity. However, it can still be difficult to resolve the structure due to limitations in spatial resolution.

In conclusion of this section, there are various methods to characterize the index of refraction change of femtosecond laser written waveguides, including near-field refractive index profilometry, etching and AFM, as well as interferometric methods. The understanding of waveguide properties and the solutions for basic mode shapes is essential toward the

optimization of experimental design and geometric layout of the structures discussed in chapters 3 and 4.

References

[1] K. M. Davis, K. Miura, N. Sugimoto, and K. Hirao, "Writing waveguides in glass with a femtosecond laser," *Optics Letters,* vol. 21, pp. 1729-31, 1996/11/01 1996.

[2] R. Osellame, V. Maselli, N. Chiodo, D. Polli, R. M. Vazquez, R. Ramponi, and G. Cerullo, "Fabrication of 3D photonic devices at 1.55 μm wavelength by femtosecond Ti:Sapphire oscillator," *Electronics Letters,* vol. 41, pp. 315-17, 2005.

[3] K. Minoshima, A. M. Kowalevicz, E. P. Ippen, and J. G. Fujimoto, "Fabrication of coupled mode photonic devices in glass by nonlinear femtosecond laser materials processing," *Optics Express,* vol. 10, 2002.

[4] C. B. Schaffer, T. N. Kim, J. F. Garcia, E. Mazur, A. Groisman, and D. Kleinfeld, "Micromachining of bulk transparent materials using nanojoule femtosecond laser pulses," Boulder, CO, USA, 2004, pp. 469-71.

[5] W. Watanabe and K. Itoh, "Fabrication of photonic devices with femtosecond laser pulses," San Jose, CA, USA, 2004, pp. 119-26.

[6] M. Richardson, A. Zoubir, L. Shah, C. Rivero, C. Lopez, K. Richardson, N. Ho, and R. Vallee, "Ablation and optical property modification of transparent materials with femtosecond lasers," Boulder, CO, USA, 2004, pp. 472-80.

[7] R. Stoian, M. Boyle, A. Thoss, A. Rosenfeld, G. Korn, and I. V. Hertel, "Laser ablation of dielectrics using ultrashort and temporally shaped laser pulses," Taos, NM, USA, 2002, pp. 135-42.

[8] A. M. Streltsov and N. F. Borrelli, "Study of femtosecond-laser-written waveguides in glasses," *Journal of the Optical Society of America B-Optical Physics,* vol. 19, pp. 2496-2504, OCT 2002.

[9] M. Will, S. Nolte, B. N. Chichkov, and A. Tunnermann, "Optical properties of waveguides fabricated in fused silica by femtosecond laser pulses," *Applied Optics,* vol. 41, pp. 4360-4364, JUL 20 2002.

[10] K. Miura, J. Qiu, H. Inouye, T. Mitsuyu, and K. Hirao, "Photowritten optical waveguides in various glasses with ultrashort pulse laser," *Applied Physics Letters,* vol. 71, pp. 3329-31, 1997/12/08 1997.

[11] S. M. Eaton, H. B. Zhang, and P. R. Herman, "Heat accumulation effects in femtosecond laser-written waveguides with variable repetition rate," *Optics Express,* vol. 13, pp. 4708-4716, JUN 13 2005.

[12] R. Osellame, S. Taccheo, M. Marangoni, R. Ramponi, P. Laporta, D. Polli, S. De Silvestri, and G. Cerullo, "Femtosecond writing of active optical waveguides with astigmatically shaped beams," *Journal of the Optical Society of America B (Optical Physics)*, vol. 20, pp. 1559-67, 2003.

[13] Y. Sikorski, A. A. Said, P. Bado, R. Maynard, C. Florea, and K. A. Winick, "Optical waveguide amplifier in Nd-doped glass written with near-IR femtosecond laser pulses," *Electronics Letters*, vol. 36, pp. 226-227, 2000.

[14] C. Mendez, G. A. Torchia, D. Delgado, I. Arias, and L. Roso, "Fabrication and characterization of Mach-Zehnder devices in LiNbO ₃ writen with femtosecond laser pulses," Mondello, Palermo, Italy, 2005.

[15] K. Minoshima, A. M. Kowalevicz, I. Hartl, E. P. Ippen, and J. G. Fujimoto, "Photonic device fabrication in glass by use of nonlinear materials processing with a femtosecond laser oscillator," *Optics Letters*, vol. 26, pp. 1516-18, 2001.

[16] J. R. Liu, Z. Y. Zhang, S. D. Chang, C. Flueraru, and C. P. Grover, "Directly writing in fused of 1-to-N optical waveguide power splitters silica glass using a femtosecond laser," *Optics Communications*, vol. 253, pp. 315-319, 2005.

[17] T. Pertsch, U. Peschel, F. Lederer, J. Burghoff, M. Will, S. Nolte, and A. Tunnermann, "Discrete diffraction in two-dimensional arrays of coupled waveguides in silica," *Optics Letters*, vol. 29, pp. 468-470, 2004.

[18] V. Sharma, A. M. Kowalevicz, Jr., R. Huber, J. G. Fujimoto, and K. Minoshima, "Three dimensional waveguide splitters fabricated in glass using a femtosecond laser oscillator," Baltimore, MD, USA, 2005.

[19] S. Nolte, M. Will, J. Burghoff, and A. Tunnermann, "Ultrafast laser processing: new options for three-dimensional photonic structures," *Journal of Modern Optics*, vol. 51, pp. 2533-2542, 2004.

[20] R. Osellame, V. Maselli, N. Chiodo, D. Polli, R. M. Vazquez, R. Ramponi, and G. Cerullo, "Fabrication of 3D photonic devices at 1.55 um wavelength by femtosecond Ti:Sapphire oscillator," *Electronics Letters*, vol. 41, pp. 315-17, 2005.

[21] K. Suzuki, V. Sharma, J. G. Fujimoto, and E. P. Ippen, "Characterization of symmetric [3x3] directional couplers fabricated by direct writing with a femtosecond laser oscillator," *Optics Express*, vol. 14, pp. 2335-2343, 2006.

[22] K. Minoshima, A. M. Kowalevicz, E. P. Ippen, and J. G. Fujimoto, "Fabrication of coupled mode photonic devices in glass by nonlinear femtosecond laser materials processing," *Optics Express*, vol. 10, 2002.

[23] P. Bado, "Manufacturing of High Quality Integrated Optical Components by Laser Direct-Write," *International Congress on Applications of Lasers and Electrooptics(ICALEO)*, 2003.

[24] M. Kamata, M. Obara, R. R. Gattass, L. R. Cerami, and E. Mazur, "Optical vibration sensor fabricated by femtosecond laser micromachining," *Applied Physics Letters*, vol. 87, pp. 51106-1, 2005.

[25] R. Osellame, S. Taccheo, M. Marangoni, R. Ramponi, P. Laporta, D. Polli, S. De Silvestri, and G. Cerullo, "Femtosecond writing of active optical waveguides with astigmatically shaped beams," *Journal of the Optical Society of America B (Optical Physics)*, vol. 20, pp. 1559-67, 2003.

[26] G. Della Valle, S. Taccheo, R. Osellame, A. Festa, G. Cerullo, P. Laporta,. "1.5 um single longitudinal mode waveguide laser fabricated by femtoseocnd laser writing" *Optics Express*, vol.15-6, 2006.

[27] G. Della Valle, R. Osellame, G. Galzerano, N. Chiodo, G. Cerullo, P. Laporta, and O. Svelto. "Passive mode locking by carbon nanotubes in a femtosecond laser written waveguide laser," *Applied Physics Letters*, vol. 89, pp. 231115, 2006.

[28] J. B. Ashcom, R. R. Gattass, C. B. Schaffer, and E. Mazur, "Numerical aperture dependence of damage and supercontinuum generation from femtosecond laser pulses in bulk fused silica," *Journal of the Optical Society of America B (Optical Physics)*, vol. 23, pp. 2317-22, 2006.

[29] C. B. Schaffer, A. O. Jamison, and E. Mazur, "Morphology of femtosecond laser-induced structural changes in bulk transparent materials," *Applied Physics Letters*, vol. 84, pp. 1441-1443, 2004.

[30] Y. Kondo, J. Qiu, T. Mitsuyu, K. Hirao, and T. Yoko, "Three-dimensional microdrilling of glass by multiphoton process and chemical etching," *Japanese Journal of Applied Physics, Part 2: Letters*, vol. 38, pp. 1146-1148, 1999.

[31] S. Juodkazis, K. Yamasaki, A. Marcinkevicius, V. Mizeikis, S. Matsuo, H. Misawa, and T. Lippert, "Microstructuring of silica and polymethylmethacrylate glasses by femtosecond irradiation for MEMS applications," Boston, MA, USA, 2002.

[32] A. Marcinkevicius, S. Juodkazis, V. Mizeikis, M. Watanabe, S. Matsuo, J. Nishii, and H. Misawa, "Fabrication of 3D interconnected network of microchannels inside silica by femtosecond irradiation and etching," San Jose, CA, USA, 2001.

[33] A. A. Said, M. Dugan, P. Bado, Y. Bellouard, A. Scott, and J. R. Mabesa, Jr., "Manufacturing by laser direct-write of three-dimensional devices containing optical and microfluidic networks," San Jose, CA, USA, 2004.

[34] J. B. Ashcom, R. R. Gattass, C. B. Schaffer, and E. Mazur, "Numerical aperture dependence of damage and supercontinuum generation from femtosecond laser pulses in bulk fused silica," *Journal of the Optical Society of America B (Optical Physics)*, vol. 23, pp. 2317-22, 2006.

[35] C. B. Schaffer, A. O. Jamison, and E. Mazur, "Morphology of femtosecond laser-induced structural changes in bulk transparent materials," *Applied Physics Letters*, vol. 84, pp. 1441-1443, 2004.

[36] R. Stoian, M. Boyle, A. Thoss, A. Rosenfeld, G. Korn, and I. V. Hertel, "Laser ablation of dielectrics using ultrashort and temporally shaped laser pulses," Taos, NM, USA, 2002.

[37] M. Richardson, A. Zoubir, L. Shah, C. Rivero, C. Lopez, K. Richardson, N. Ho, and R. Vallee, "Ablation and optical property modification of transparent materials with femtosecond lasers," Boulder, CO, USA, 2004.

[38] D. Gomez, I. Goenaga, I. Lizuain, and M. Ozaita, "Femtosecond laser ablation for microfluidics," *Optical Engineering*, vol. 44, pp. 51105-1, 2005.

[39] C. Pollock, M. Lipson. Integrated Photonics Springer Press, New York. 2003.

[40] K. Okamoto. Fundamentals of Optical Waveguides. Elsevier, Burlington. 2006.

[41] C. Florea and K. A. Winick, "Fabrication and characterization of photonic devices directly written in glass using femtosecond laser pulses," *Journal of Lightwave Technology,* vol. 21, pp. 246-253, JAN 2003.

[42] D.P.Dave and T.E. Milner, "Refractive index profiling of embedded microstructures in optical materials," *Applied Optics,* vol. 41-10, 2002

[43] R. S. Taylor, C. Hnatovsky, E. Simova, D. M. Rayner, V. R. Bhardwaj, and P. B. Corkum, "Ultra-high resolution index of refraction profiles of femtosecond laser modified silica structures," in *Conference on Lasers and Electro-Optics (CLEO), Conference on Lasers and Electro-Optics (CLEO) (IEEE Cat. No.CH37419-TBR)*. Baltimore, MD, USA: Optical Soc. of America, 2003.

[44] R. Gattass, L. Cerami, E. Mazur. "Micromachinning of builk glass with bursts of femtosecond laser pulses at variable repetition rates." *Optics Express* 14-12. 2006.

CHAPTER 2: DEVICE FABRICATION AND MEASUREMENT

2.1 Fabrication Setup

For ideal device fabrication, it is necessary to have high precision positioning of the sample relative to the writing source, preferably with position accuracy on the wavelength scale. In addition, it is necessary to develop a writing source which produces waveguides in a regime where there is symmetric waveguide profile and low loss. Specific writing parameters, such as focusing depth and scanning speed are determined by the writing source and scanning equipment available. Fig. 1 shows a diagram of the fabrication setup.

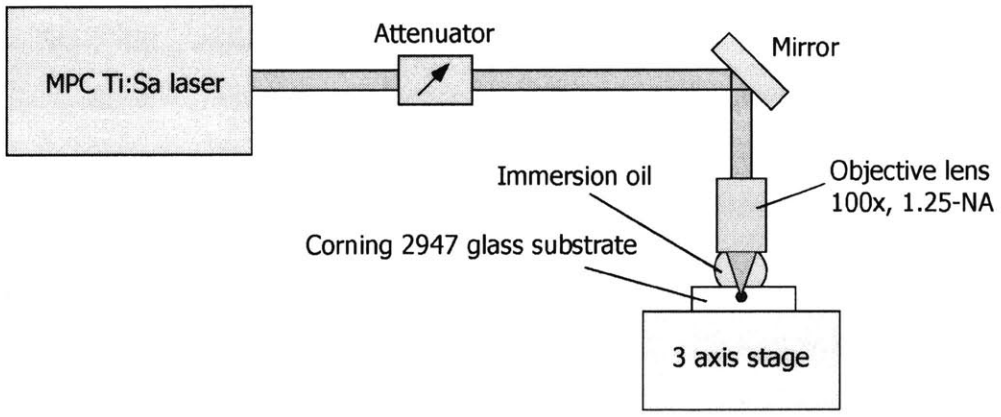

Fig. 1. Waveguide fabrication setup. This is the identical setup used in ref [1]

In most experimental setups, it is common to use a high accuracy, 3-axis stage[2,3]. Likewise in our experiment, the substrate was translated in a direction orthogonal to that of the propagating beam using a high-precision floating 3 axis stage (Aerotech ABL1100) controlled using standard CNC code (G code). The sample is translated using XY(ABL-125820) and Z stage(ABL-135895). The XY stages are air-bearing and frictionless with centimeter scale travel, and the Z stage is a mechanical wedge stage with around 2 mm travel. The writing source is a novel Multiple-pass Cavity (MPC) Ti:sapphire oscillator- to be described in the next section -and is attenuated so the exposure at the sample is around 120 mW to ensure single-mode operation, then focused with an oil-immersion 100X Olympus 1.25 NA onto the substrate. The scan speed

is between 10 and 12 mm/s. Single mode operation is chosen by measuring the output waveguide intensity profile by translating a SMF fiber at the output and by observing the output intensity with a CCD camera. Writing speeds are chosen to ensure single-mode operation while keeping losses relatively low.

Since waveguide structures need to be controlled to a high degree of accuracy, the air-bearing stage from Aerotech is chosen for its high position (10 nm) and velocity accuracy (0.001 mm/s). The stage is operated using an optical feedback encoder interpolator which gives the controller a position reading with a feedback cycle of around 100 kHz. The CNC code which controls the machine is directly compiled on the controller and fed through the encoder to the stage. CNC code is standard machine code and waveguides are created using commands for linear and circular motion. The Aerotech computer firmware and software operates as an equivalent real-time operating system. Details about the control system for stage operation will be discussed further in chapter 5.

Since focusing is performed at high NA, a layer of index matching immersion oil is spread on the sample. The beam is focused around 500 um below the surface of the substrate using a 100x objective to ensure waveguides are fully embedded. The beam focus is translated manually below the sample surface until plasma generation can be observed. During fabrication, the stage is commanded to move the beam focus and additional 300 um down into the substrate. Since the index modification process is based on nonlinear absorption, device writing can be performed at different depths inside the material without causing collateral damage. However, for the devices discussed in the current study, all fabrication is performed at a constant depth.

Two different substrates were used in the course of this study. At first Corning 2497 microscope objective slides were used, then the Corning EAGLE^{2000} display glass was chosen for its favorable thermal properties. EAGLE glass is a LCD display glass known for its low density (2.3 g/cm^3) and high thermal stability (31.8x10^{-7}/°C CTE). EAGLE glass resulted in waveguides with lower insertion loss compared with the previous substrate, and desirable coupler characteristics have already been measured from devices fabricated in this substrate [4].

2.2 Novel Multiple-pass Cavity Ti:Sapphire Laser

Because waveguide properties such as mode size and index of refraction are sensitive to both the exposure power and scanning speed, it is important to explore the threshold for high-speed femtosecond laser waveguide fabrication. To this end, it is essential to develop specialized laser sources for meeting the needs of the experiment. Kowalevicz et al.[5] developed a novel compact Kerr-lens modelocked femtosecond Ti: Sapphire laser based on a novel multipass cavity (MPC), which was used to fabricate all devices in this study. The MPC laser generates 45 fs duration pulses with 150 nJ of energy per pulse [5]. The extended cavity reduces the laser repetition rate from about 100MHz to 5.85 MHz, scaling the output pulse energy accordingly.

In contrast to amplified femtosecond systems, the MPC laser has a repetition rate high enough to produce an accumulated heating effect which enables device fabrication approximately three orders of magnitude faster than possible using amplified systems. Moreover, MHz-range repetition rate lasers are advantageous for fabricating waveguide devices since the photomodification is caused mainly by thermal diffusion, resulting in symmetric waveguide cross-sections, while kHz repetition rate lasers can cause elliptical or non-symmetric cross-sections due to nonlinear absorption and plasma [2]. Finally, the relatively high energy generated by the MPC laser system enables waveguide fabrication to be performed with fewer constraints on the numerical aperture, giving greater flexibility and versatility to the writing process. Fig. 2 shows the layout of the MPC Ti:sapphire laser [5].

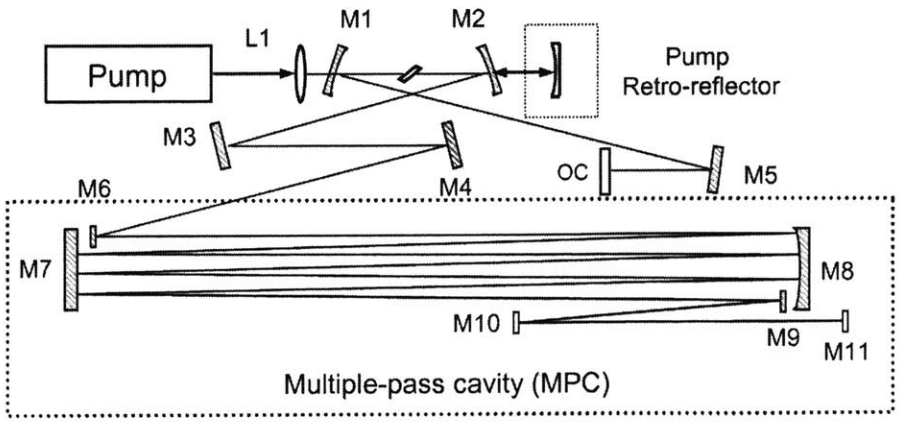

Fig. 2 from ref [5] Schematic layout of MPC Ti:sapphire laser. The MPC is composed of M7 and M8.

The MPC laser is based on the idea of extending the length of one arm while preserving the q parameters of the Gaussian beam so that the stability and KLM characteristics of the long cavity is similar to that of the short cavity. The short cavity is based a on a standard X-folded configuration for Ti:sapphire lasers which is shown in Fig. 3, reprinted from ref [7].

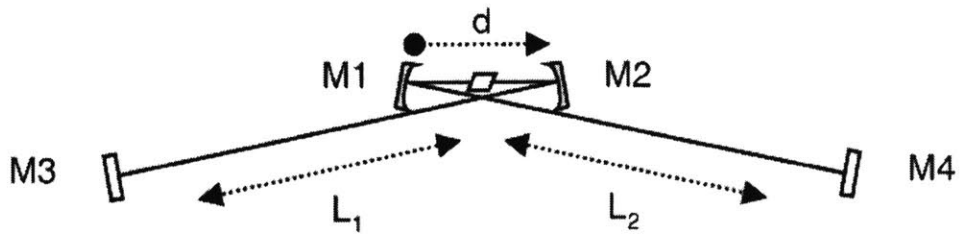

Fig 3. from ref [7] Schematic of standard X-folded KLM Ti:sapphire laser cavity

The arms lengths of the two legs (L_1, L_2) are asymmetric and are measured to be 45 cm and 95 cm, respectively. Based on this cavity, it is possible to calculate the kerr lens sensitivity, a parameter which measures the stability of mode-locking, as a function of crystal position and curved mirror separation. Fig 4 from ref [8] shows a typical calculation for arm lengths of 50cm and 110 cm.

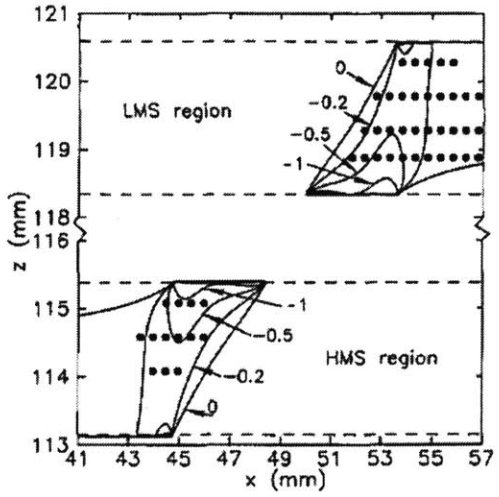

Fig. 4 from ref [8]. Kerr lens sensitivity as a function of crystal position(x) and curved mirror separation(z). KLM can be initiated in solid circles.

Introducing an MPC is a method for scaling up pulse energies while maintaining the original characteristics of the X-folded cavity without the need for expensive and complex amplifier systems. The MPC should extend the length of the cavity while preserving the KLM stability map and operating point [9]. The beam is introduced into the MPC by M6 and makes 12 passes through the unit cell. Q preservation requires that the total transformation experience by the beam inside the MPC must be unity. This can be satisfied by examining the ABCD matrix for each unit cell. The unit cell is defined as a propagation distance d, a lens with focal length f, and another propagation of length d. If the MPC consists of N unit cells, then the Nth power of the matrix must be 1. This is shown in equation (1) below from ref [5].

$$\begin{bmatrix} 1 & d \\ 0 & 1 \end{bmatrix}\begin{bmatrix} 1 & 0 \\ -1/f & 1 \end{bmatrix}\begin{bmatrix} 1 & d \\ 0 & 1 \end{bmatrix}$$
$$= \begin{bmatrix} 1 - d/f & 2d - d^2/f \\ -1/f & -d/f + 1 \end{bmatrix}$$
$$\Rightarrow \begin{bmatrix} 1 - d/f & 2d - d^2/f \\ -1/f & -d/f + 1 \end{bmatrix}^N = \pm 1 . \quad (1)$$

In the current design, the cavity has N=12. The calculated focal length of the M8 mirror is 7.5 m and the distance between mirrors is 1 m. M11 is flat and the beam is retroreflected back to the reference position with the q parameter approximately the same.

After optimizing for KLM operation, the beam from the output coupler of the laser source is focused using immersion oil, onto the substrate mounted to the translation stage. For our particular experiment, power before the objective lens is ~180 mW. Fig. 5 below shows (a) back-ground free second-harmonic autocorrelation measurements showing a 67 fs FWHM accounting for the sech squared pulse shape. (b) the long-cavity output spectrum of the MPC laser and (c) the fast photodiode pulse trace showing 171 ns between pulses.

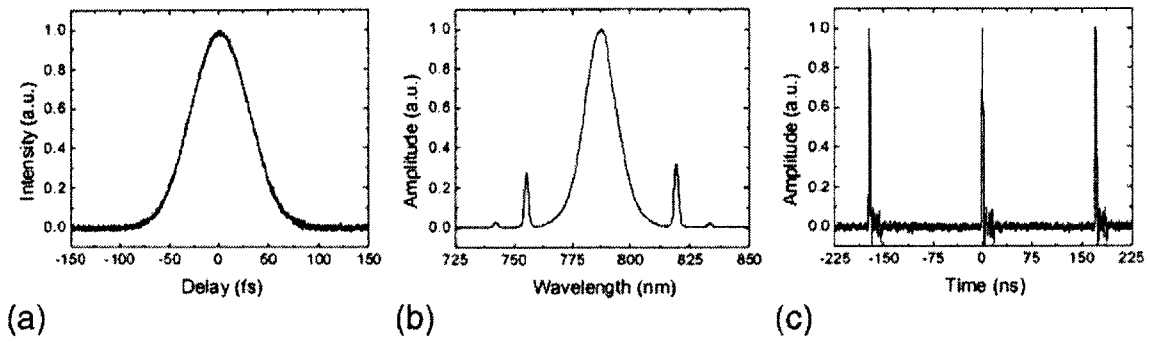

Fig. 5 from ref [5] (a) back-ground free second-harmonic autocorrelation measurements showing a 67 fs FWHM (b) the long-cavity output spectrum of the MPC laser and (c) the fast photodiode pulse trace showing 171 ns between pulses.

The spectrum has a FWHM of 16.5 nm centered at 788. The narrow, symmetric sidebands are Kelly sidebands which result from phase matching with the soliton continuum. The second harmonic autocorrelation trace was performed with a 300 um thick KDP crystal. Using an assumed secant squared pulse shape, the autocorrelation trace yields a pulse length of 43 fs, which is close to the calculated transform limited pulse length of 39 fs. The typical laser output power noise was less than 5%. For our experiments, the throuput of the objective was around 70% and the power was attenuated so power at the sample was around 120 mW.

2.3 Measurement

Scan speed for lower repetition rate systems can be as low as 20 um/s, while the upper range for scanning speed is usually 12-20 mm/s. An earlier investigation of waveguide fabrication in our group characterized the waveguide size as well as index change with respect to scan speed. For EAGLE glass substrate, a similar set of experiments were performed. Straight waveguide were written with speeds varying between 4 mm/s and 20 mm/s. Since there is a clear correlation between the diameter of the structure and the writing speed, a suitable choice for writing speed enables high speed scanning while maintaining single mode operation with relatively low loss. Insertion loss and output intensity profiles were measured for each waveguide. From the intensity profile it can be verified whether the device is single or multi-mode. Single-mode operation was verified by observing the output using a CCD camera. Fig. 6 shows a single mode intensity output profile from a waveguide written at 12 mm/s with 2.1 mW of 1550 nm light coupled in via single mode fiber.

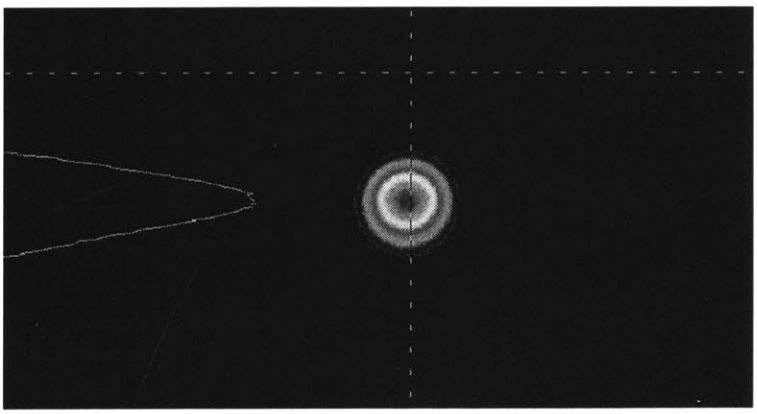

Fig. 6. Output intensity profile for single mode waveguide written at 120 mW power and 12 mm/s. The input is 2.1 W of 1550 nm light coupled in through single mode fiber.

Approximate mode size was measured by translating a SMF at the output of the device in um scale increments. For scanning speeds of 10-20mm/s, the FWHM of the output mode size was observed to be smaller than the FWHM of the output mode measured using the same technique for a single mode fiber.

For couplers and interferometric devices, it is necessary to confirm structures are smooth and continuous using a phase contrast microscope at high magnification (40x). After verifying the desired waveguides structures, the input and output facets are polished to <3um smoothness. To characterize spectral features, light from a tunable laser source (Santec TSL-210 1500 to 1600nm) is coupled into the waveguide using single-mode fiber. Coupling loss is estimated to be 2-3 dB per interface. To reduce coupling loss, the ends of the sample are polished and index-matching oil is applied. Fig. 5 shows a diagram of the measurement setup.

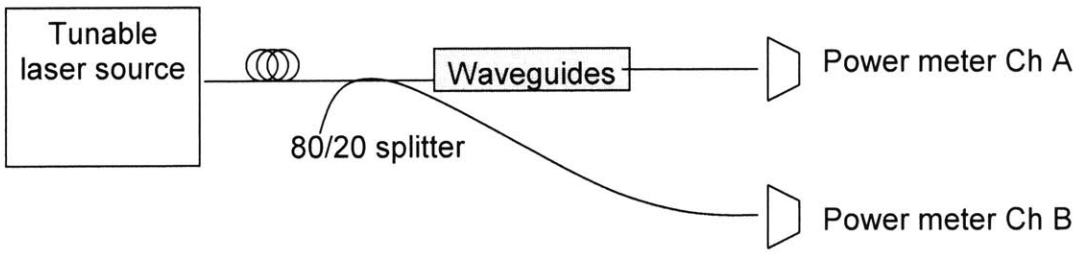

Fig. 5. Diagram representation of measurement setup. Power measurements are made as the ratio ChA/ChB.

To normalize the output against losses in real-time, a fraction of the power from the tunable laser source is sent directly to a second power meter, and the measurement is taken as a ratio of the power at the output of the device with the power measured in the second power meter. Matlab is used to interface between the GPIB boards connected to the tunable laser source and the digital read out from the power meter. To reduce instabilities in the tunable laser source, there is a pause of 3 seconds after the initial wavelength tuning to 1500 nm, and 10 measurements are taken at each wavelength and averaged over. All measurements on each sample are normalized with respect to a straight waveguide on that particular sample.

Because femtosecond micromachining enables the writing of three-dimensional structures, it is important to have a reliable technique for imaging and characterizing three-dimensional waveguide structures. As mentioned earlier, OCT imaging techniques can be used to generate three-dimensional images of small changes in index of refraction. We have developed a novel rapidly tunable narrowband "swept source" Fourier Domain Modelocking (FDML) laser capable of providing greater than 100 nm tuning range at up to 370 KHz sweep rate [10]. This source can be used for rapid acquisition of three-dimensional OCT images of a large number of

complex laser micro-machined devices. The same source can also be used to measure the wavelength-dependent transfer functions of interferometric devices.

References

[1] K. Minoshima, A. M. Kowalevicz, E. P. Ippen, and J. G. Fujimoto, "Fabrication of coupled mode photonic devices in glass by nonlinear femtosecond laser materials processing," *Optics Express,* vol. 10, 2002.

[2] S. M. Eaton, H. B. Zhang, and P. R. Herman, "Heat accumulation effects in femtosecond laser-written waveguides with variable repetition rate," *Optics Express,* vol. 13, pp. 4708-4716, JUN 13 2005.

[3] S. Nolte, M. Will, J. Burghoff, and A. Tunnermann, "Ultrafast laser processing: new options for three-dimensional photonic structures," *Journal of Modern Optics,* vol. 51, pp. 2533-2542, NOV-DEC 2004.

[4] S. M. Eaton, W. Chen, L. Zhang, H. Zhang, R. Iyer, J. S. Aitchison, and P. R. Herman, "Telecom-band directional coupler written with femtosecond fiber laser," *IEEE Photonics Technology Letters*, vol. 18, pp. 2174-6, 2006.

[5] A. M. Kowalevicz, A. T. Zare, F. X. Kartner, J. G. Fujimoto, S. Dewald, U. Morgner, V. Scheuer, and G. Angelow, "Generation of 150-nJ pulses from a multiple-pass cavity Kerr-lens mode-locked Ti : Al2O3 oscillator," *Optics Letters*, vol. 28, pp. 1597-1599, 2003.

[6] K. Minoshima, I. Hartl, E. P. Ippen, and J. G. Fujimoto, "Versatile photonic device fabrication using nonlinear processing in glass with a femtosecond laser oscillator," paper presented at Conference on Lasers and Electro-Optics (CLEO), Baltimore, MD, USA, 2001.

[7] A. M. Kowalevicz . Novel Femtosecond Laser Development with Applications in Biomedical Imaging and Photonic Device Fabrication. PhD. Thesis. MIT. May 2004.

[8] G. Cerullo, S. De Silvestri, V. Magni, and L. Pallaro, "Resonators for kerr-lens mode-locked femtosecond ti:sapphire lasers," *Optics Letters*, vol. 19, no. 11, pp. 807{809, 1994.

[9] A. Sennaroglu, A.M. Kowalevicz, F.X. Kaertner, E.P. Ippen, and J.G. Fujimoto, "Novel compact femtosecond lasers based on multi-pass cavities," *IEEE Journal of Quantum Electronics*, 2003.

[10] Buffered Fourier domain mode locking: unidirectional swept laser sources for optical coherence tomography imaging at 370,000 lines/s Huber, R. (Dept. of Electr. Eng., Massachusetts Inst. of Technol., Cambridge, MA, USA); Adler, D.C.; Fujimoto, J.G. *Optics Letters*, v 31, n 20, 15 Oct. 2006, p 2975-7

CHAPTER 3: DIRECTIONAL COUPLERS

3.1 Background and existing work

3.1.1 Introduction

Photonic devices such as splitters and coupled mode devices are the building blocks of more complex devices which are of interest in many applications in telecommunications, integrated electro-optics, and sensing. X-couplers with 1:1 and 16:1 power splitting ratios were fabricated by our group at MIT using a novel MPC Ti:sapphire oscillator[1]. 1 x 2 optical splitters with ~6.55 dB insertion loss that can be cascaded into 1 x n splitters have also been demonstrated [2], and excess losses introduced by the Y junctions were substantially reduced using a double scan technique. Cubic lattices of straight waveguides have been shown to demonstrate discrete diffraction behavior through evanescent coupling, creating an effective 1-to-n splitter[3]. The fabrication of various 2 x 2 couplers has also been shown[4,5]. It is important to understand the design and characterization of directional couplers so that more complex devices, such as interferometers and filters can be built. It is important to understand the design and characterization of directional couplers so that more complex devices such as interferometers and filters can be built.

3.1.2 Coupled mode theory

To accomplish the optimal design for directional couplers it is important to understand the basics of coupled mode theory[6]. The upper and lower ports can be represented as A and B.

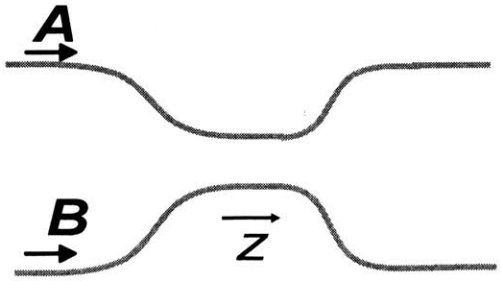

Fig 1. Schematic of directional coupler. A and B represent the upper and lower ports. The waves are modeled using $A(z) = a_1$ and $B(z) = a_2$,

As a convention, the waves in the waveguides can be modeled using $A(z) = a_1$ and $B(z) = a_2$, which, without coupling, would independently propagate with constants β_1 and β_2, as shown in below:

$$\begin{aligned} \frac{da_1}{dz} &= -j\beta_1 a_1 \\ \frac{da_2}{dz} &= -j\beta_2 a_2 \end{aligned} \tag{3.1}$$

The coupling constant, represented by κ_{12} creates a change in the propagation equation as shown:

$$\begin{aligned} \frac{da_1}{dz} &= -j\beta_1 a_1 + \kappa_{12} a \\ \frac{da_2}{dz} &= -j\beta_2 a_2 + \kappa_{12} a \end{aligned} \tag{3.2}$$

Considering co-directional propagation with nonzero input in both $a_1(0)$ and $a_2(0)$, the general solution is shown as:

$$\begin{aligned} a_1(z) &= \left[a_1(0)\left(\cos\beta_0 z + j\frac{\delta}{2\beta_0}\sin\beta_0 z \right) + \frac{\kappa_{12}}{\beta_0} a_2(0)\sin\beta_0 z \right] \cdot e^{-j[(\beta_1+\beta)_2/2]z} \\ a_2(z) &= \left[a_2(0)\left(\cos\beta_0 z + j\frac{\delta}{2\beta_0}\sin\beta_0 z \right) + \frac{\kappa_{21}}{\beta_0} a_1(0)\sin\beta_0 z \right] \cdot e^{-j[(\beta_1+\beta)_2/2]z} \end{aligned} \tag{3.3}$$

Where $\beta_0 = \sqrt{\frac{\delta^2}{4} + |\kappa_{12}|^2}$ and $\delta = \beta_1 - \beta_2$ is the propagation constant mismatch.

With the assumption of degenerate coupling constants and non-zero input only in the a_1 port, the output fields simplify to:

$$\begin{aligned} a_1(z) &= a_1(0)\left(\cos\beta_0 z + j\frac{\delta}{2\beta_0}\sin\beta_0 z \right) \\ a_2(z) &= \frac{\kappa_{21}}{\beta_0} a_1(0)\sin\beta_0 z \end{aligned} \tag{3.4}$$

In the above equations the propagation in z has been removed for simplicity. The equations show the expected behavior of co-directional coupled modes where there is a finite propagation constant mismatch δ. This mismatch causes the contrast ratio to deviate from 1. In the most

simplified approach the propagation constants are assumed to be degenerate and one can recover the standard sinusoidal coupled mode behavior:

$$\begin{aligned} a_1(z) &= a_1(0)\cos\kappa z \\ a_2(z) &= a_1(0)\sin\kappa z \end{aligned} \tag{3.5}$$

Here, the coupling constants are identical, or $\kappa = \kappa_{12} = \kappa_{21}$. It is important to note the coupling coefficient is one of the most sensitive parameters in this study. It is described by the overlap of the modes between modes in the adjacent waveguides:

$$\kappa \prec \int NA^2 \varepsilon_a(x)\varepsilon_b(x)dx$$

Where $\varepsilon_a(x)$ and $\varepsilon_b(x)$ represent modes in the transverse modes in adjacent waveguides.

κ depends nonlinearly on the waveguide separation since the mode intensities decrease exponentially with distance. Fig. 2 illustrates the concept of the coupling coefficient's dependence on interaction separation.

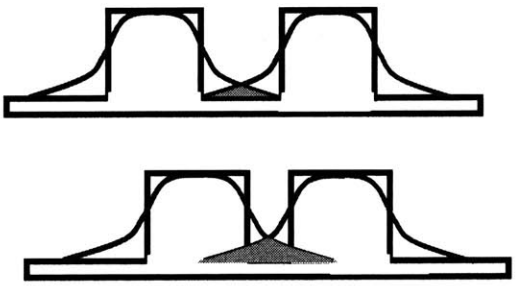

Fig. 2. The dependence of κ, represented in blue, on interaction separation. As the interaction separation is decreased, κ increases nonlinearly.

3.1.3 Curved waveguide theory

The symmetric couplers used in this study were designed to have curved segments connected to straight segments to reduce possible losses from sharp bends in the waveguide. However, with the usage of bent waveguides it is important to understand their properties.

A number of different methods have been applied to the analysis of losses in bent waveguide structures. Heiblum and Harris [7] used conformal mapping to transform a curved waveguide

into a straight structure to solve for the mode shape and propagation. In this method, a bent planar waveguide can be modeled using the Effective Index Method (EIM) as a curved two-dimentional waveguide in the plane containing the propagation. TE and TM boundary conditions are used to find the effective index of the structure. Unlike ideal straight waveguides, in bent waveguides, the phase relation for the guided optical field is not constant along the direction of propagation. Considering the physics of total internal reflection, within a bent waveguide each reflection on the outer waveguide boundary produces some loss of the guided field. This loss is represented by the imaginary part of the propagation constant β. It has been theoretically shown that the bending loss for a 90° bend with circular radius of curvature R_2 can be given as. $4.342 \cdot \pi \cdot R_2 \, \mathrm{Im}(\beta)$ dB [8]. For consistency note that the imaginary part of β is zero for a straight waveguide, meaning there is no loss purely as a result of propagation. Fig. 3 from ref [8] shows the transformation of index profile, which is a conformal transformation of the *xy* plane into the *uv* plane.

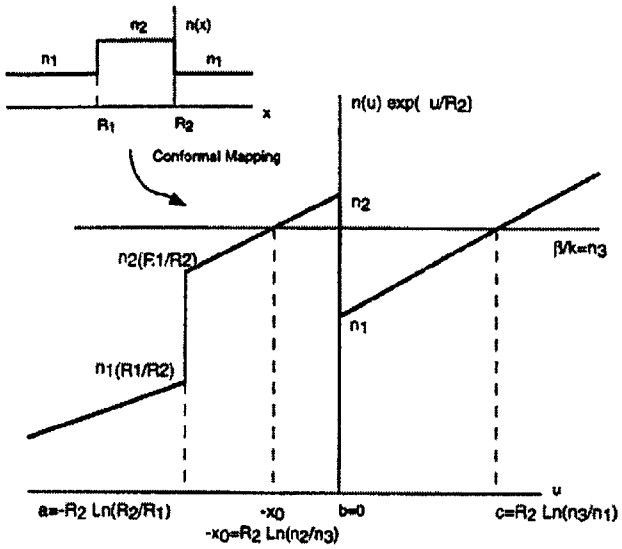

Fig 3 from ref [8] the transformation of index profile from a bend waveguide to a straight waveguide with effective non-uniform index. This is a conformal transformation of the "x-y "plane into the "uv" plane.

The propagation of the E and H field can be solved in *uv* space, along with appropriate boundary conditions. The equations are reprinted from [8].

$$\frac{d^2E_z}{du^2}+\left(k^2{n_{TM}}^2\exp\left(\frac{2u}{R_2}\right)-\beta^2\right)E_z=0$$
$$\frac{d}{du}\left(\frac{1}{{n_{TM}}^2}\frac{dH_z}{du}\right)\left(k^2\exp\left(\frac{2u}{R_2}\right)-\frac{\beta^2}{{n_{TE}}^2}\right)H_z=0 \tag{3.6}$$

at the discontinuities u_o, the mode must satisfy boundary conditions

$$TE\begin{cases}E_z(u_0)\big|_-^+=0\\ \dfrac{dE_z(u_0)}{du}\Big|_-^+=0\end{cases}$$
$$TM\begin{cases}H_z(u_0)\big|_-^+=0\\ \dfrac{1}{n_{TE}^2}\dfrac{dH_z(u_0)}{du}\Big|_-^+=0\end{cases}$$
$$\text{defining } f(u_0)\big|_-^+=f(u_0^+)-f(u_0^-) \tag{3.7}$$

The mode solutions are found using the WKB method. A pictorial of the transverse mode is shown in Fig. 4 from [8]. The mode is pushed out toward the outer curve of the bent waveguide and power is radiating away, resulting in loss.

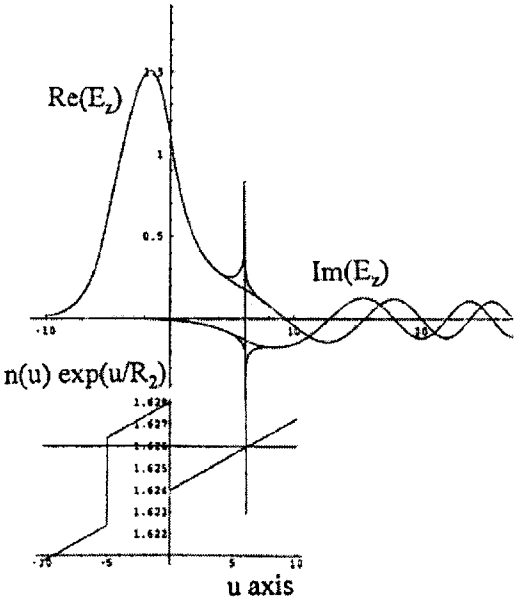

Fig 4 from ref [8]. The solution to the transverse mode using WKB analysis shown with a graph of the effective refractive index.

It is clear that bending loss is dependent on the radius of curvature, with smaller radii creating larger losses. Kiremath *et al* demonstrated this using a rigorous classical analytic frequency

domain model of guided wave propagation using mode profiles based on Bessel and Hankel functions. From Fig. 5 in [9] it can be seen that structures with smaller radii have more oscillation in the solution of the E field toward the waveguide's outer edge. Thus, more energy is radiated, causing greater losses.

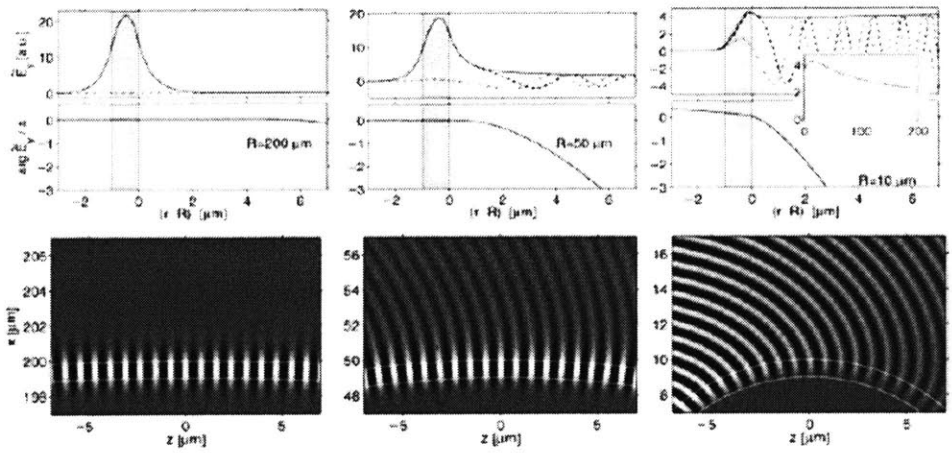

Fig 5 from ref [9]. Analytical models of the TE_{00} mode for radii of 200, 50 and 10 um. Smaller radii result in more significant loss.

3.1.4 Existing work

Several groups have already demonstrated the fabrication of asymmetric and symmetric directional couplers. An earlier study conducted in our group demonstrated the fabrication of asymmetric directional couplers [4]. Devices were fabricated using the extended cavity Ti:Sapphire oscillator, as described in chapter 2, with pulse energies of about 20 nJ and scan speeds of 10 mm/s. Figure 6 from [4] shows (a) the phase-contrast microscope picture of the directional coupler and (b) the schematic of the directional coupler showing the interaction length.

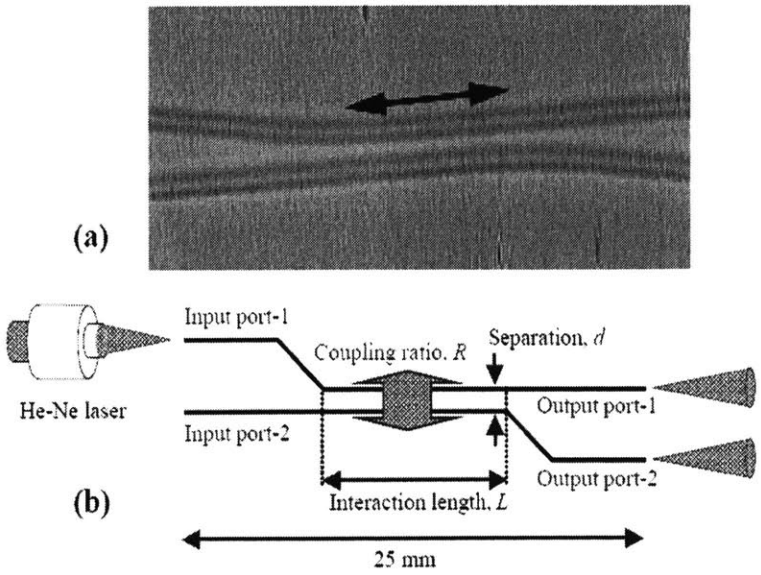

Fig 6 from ref [4]. (a) Phase contrast microscope image of asymmetric directional coupler. And (b) schematic of coupler design showing interaction length L and separation d [4]

For the above couplers, the through port coupling ratio was measured while varying the interaction length L and separation distance d. Figure 7 from [4] shows the variation of coupling ratio with respect to the interaction length L for separation values of 8, 10, and 12 um.

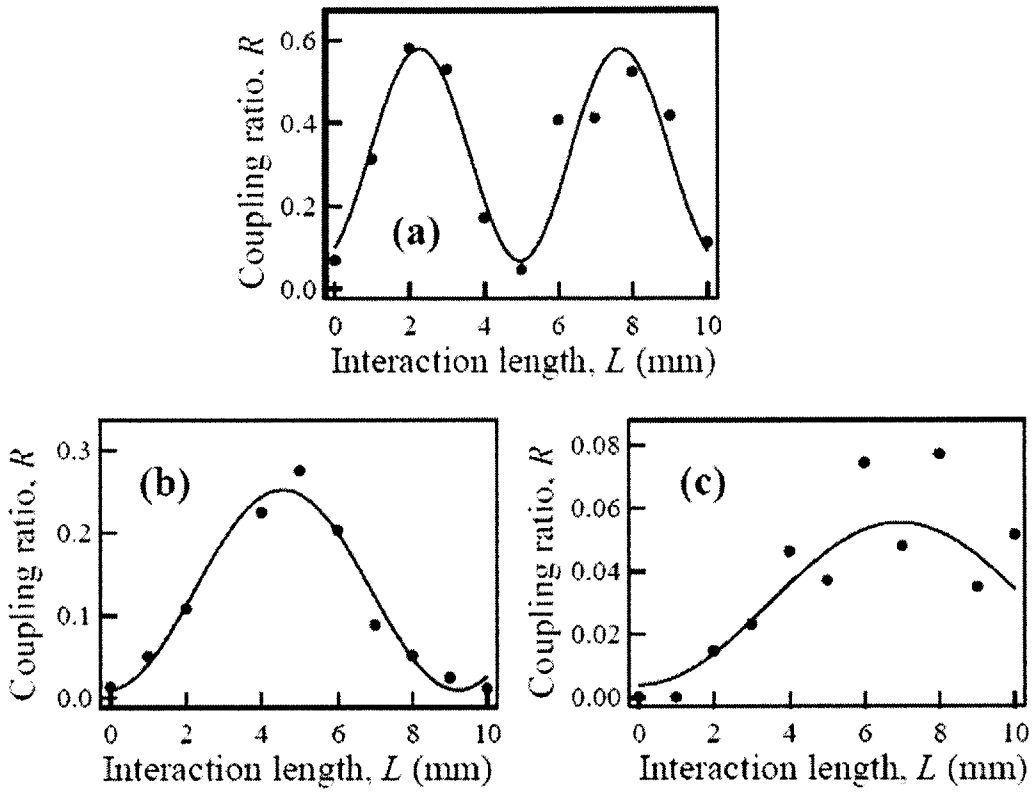

Fig 7 from ref [4]. Coupling ratios with interaction lengths of 0 to 10 mm, with interaction separations of (a) 8um, (b) 10um, and (c)12um. The smooth curve shows theoretical behavior.

As expected, the coupling ratio varies more rapidly for smaller interaction separations and more gradually for increased interaction separations. This is consistent with the theory that a decrease in the coupling coefficient results in an increase in the oscillation period of the coupling ratio with interaction length. The errors between the theoretical and experimental data are due to measurements being made on different devices. This means there could have been variations in the coupling of the input beam into each device and micron scale fluctuations in interaction separation. The variation in coupling ratio from measurement errors was estimated to be $\pm$ 0.02. For the longest interaction length, the scatter in data is greater due to the measurement of a weak signal. Another important point to note is that the contrast ratio in the experimental data does not reach unity and decreases with increasing waveguide separation. This implies there is a mismatch in propagation constants between the two waveguides due to fabrication error.

In the same study, the first spectral characterization of femtosecond laser fabricated directional couplers was performed. The spectral characteristic of the coupling ratio is shown in figure 8 from [4].

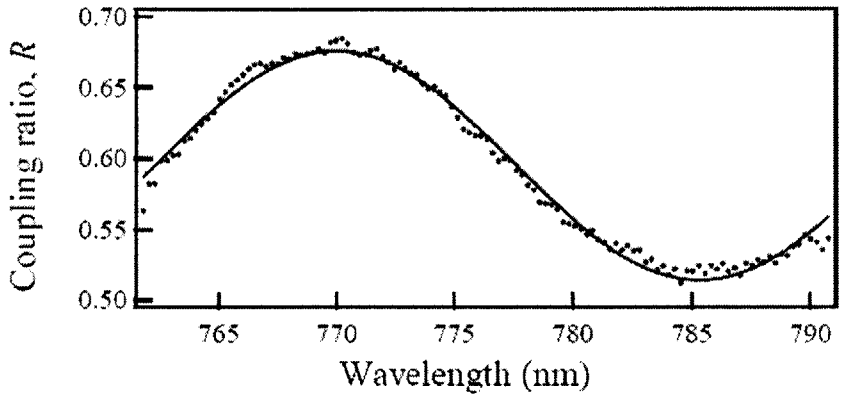

Fig 8 from ref [4]. The wavelength dependence of coupling ratio centered around 775 nm.

As will be discussed later in this chapter, spectral measurements are important because they show the variation of coupling coefficient with wavelength. In addition, they allow for multiple measurements to be made on a single sample, eliminating variations from measurement of different devices. From the current measurement, it can be seen that the coupling ratio varies sinusoidaly with wavelength as expected, but there is a large wavelength-independent background signal resulting from scattered light detected from the spectrometer. This study shows the concept of characterizing the spectral behavior of devices fabricated with a femtosecond laser, although there can be improvements made on the measurement system itself to reduced background noise.

In 2004, Liu *et al*, also demonstrated symmetric 1 x 2 and 2 x 2 waveguide directional couplers [10]. Fig. 9 shows the schematic layout of the 1 x 2 and 2 x 2 couplers, respectively. Couplers are symmetric and consist of *s*-shaped curves with 225 mm bending radius.

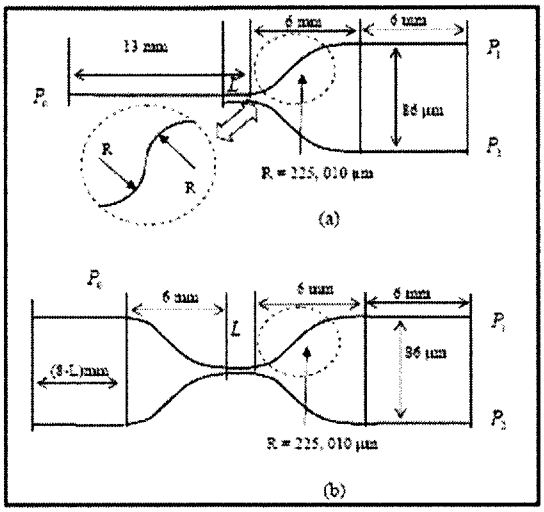

Fig 9 from ref [10]. The schematic layout of the 1x2 and 2x2 couplers. Couplers are symmetric and consist of s shaped curves with 225 mm bending radius.

By writing a series of 1 x 2 directional couplers, the coupling coefficient was calculated. 3 dB directional couplers were optimized for the wavelength of 1.5 um. The multi-scan technique, with a shift in the second write, was used to reduce losses in the *s* bends. It is speculated that multi-scanning modifies the index change and profile shape of the waveguides in the bent region to reduce loss. The insertion loss and polarization dependent losses for the couplers at 1.5 um were measured to be 6.55 $\pm$0.25 dB and 0.28$\pm$0.12 dB respectively.

Following previous studies, telecom-band directional couplers written with a 1 MHz femtosecond fiber laser were demonstrated [11]. Waveguides were fabricated with a commercial femtosecond fiber laser (IMRA) with 400 fs pulses at 1045 nm inside Corning EAGLE^{2000} borosiliacte glass, producing low-loss (0.3 dB/cm), directional couplers with three different interaction separations - 7.5 um, 12.5 um, and 17.5 um. As shown in Fig. 10 from [11], the thru port coupling ratios have a periodic dependence on interaction length and have high extinction ratios for the telecom wavelengths 1300 nm and 1550 nm.

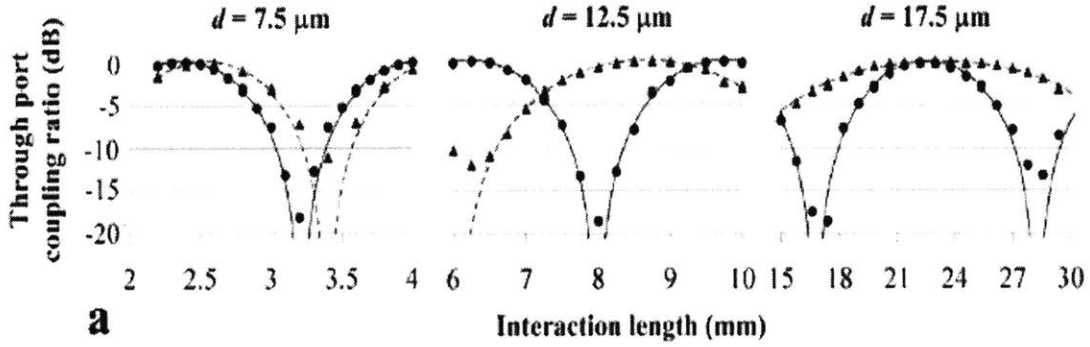

Fig 10 from ref [11]. Through port coupling ratios of telecom band directional couplers as function of interaction length for difference interaction separations d (7.5um,12.5um and 17.5um). Triangles indicate data for 1310 nm; Solid circles indicate data for 1550 nm.

The data presented above is improved from previous data as the contrast ratio approaches unity and follows the expected sinusoidal response quite closely. At 1550 nm, the maximum coupling ratio is estimated to be around 99%. At 1330 nm, the contrast ratio is smaller and estimated to be around 93%. It is hypothesized that the coupling behavior is improved from earlier results from our group because waveguides have identical radii of curvature and, therefore, more closely matched propagation constants. The insertion loss was about 2 dB.

There is existing data demonstrating the periodic behavior of the coupling ratio shown by varying the interaction length, and it has been shown that the period of the coupling ratio varies with interaction separation. The goal for the current study was to perform a detailed characterization of the wavelength dependence of femtosecond laser fabricated directional couplers and to show that (a) the wavelength characteristics can be tailored for specific needs by controlling the physical parameters of the devices such as interaction length, waveguide separation, and radius of curvature, and (b) it is possible to achieve wavelength-independent 3dB couplers which would enable the building of more complex structures.

3.2 Design of Symmetric Directional Couplers

3.2.1 Design considerations

The two main parameters for directional coupler design are interaction length and waveguide separation in the interaction region. The optimal design for the symmetric directional coupler is one in which the interaction waveguide separation is minimized, which minimizes deviations from ideal coupling behavior caused by stage position errors. Since the waveguide size is estimated to be 3-5 um wide, the interaction separation was set at 5 um. Phase contrast microscopy was used to check that waveguides were not overlapping.

Bending loss and wavelength-dependent bending loss determine the appropriate choice of bend radius. Experimentally, Eaton *et al.* characterized the bending loss of waveguides fabricated using a femtosecond laser source as function of bend radii, shown in figure 11 from [11].

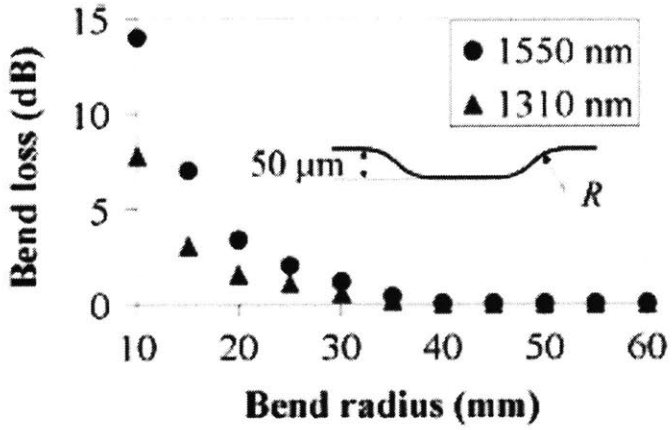

Fig 11 from ref [11]. Bending loss as a function of bend radius at 1550 nm and 1310 nm.

From this data it can be seen that above a certain radius threshold, bending losses are well matched with straight waveguide losses. However, below the threshold bending loss is exponentially dependent upon bend radius. In addition, bending loss seems to be greater at the longer wavelength of 1550 nm.

It is important to understand how the loss due to bending in the waveguide is wavelength dependent. It is intuitive that longer wavelengths see a sharper bend and therefore experience

more loss. Heiblum showed that the attenuation constant α is proportional to an exponential dependence on wavelength [7]:

$$\alpha \prec \exp\left(-\frac{4\pi}{\lambda} R_2 n_3 \delta\right)$$

$$\text{with the mode } \Psi(u,v) \prec F(u)\exp[i(\beta + i\alpha)v] = F(u)\exp[i(\beta + i\alpha)R_2\theta]$$

$R_2\theta$ defines the distance in the direction of propagation. Therefore, in theoretical models, bending loss is expected to be nonlinearly dependent on wavelength.

From experimental results on our current waveguides it can be seen that wavelength dependence of bending loss can be significant for radii smaller than 60 mm. The wavelength dependent loss in a bend is larger at longer wavelengths and smaller at shorter wavelengths, causing a monotonic decrease in power in measurements taken from the previous coupler design. Fig. 12 below shows the wavelength data of the transmission through an *s*-shaped bend created using two circular segments of waveguide with radius of curvature of 23.6 mm. The power after the objective was 120 mW and writing speed was 12 mm/s. The wavelength dependent loss causes the power to decrease by approximately 80%.

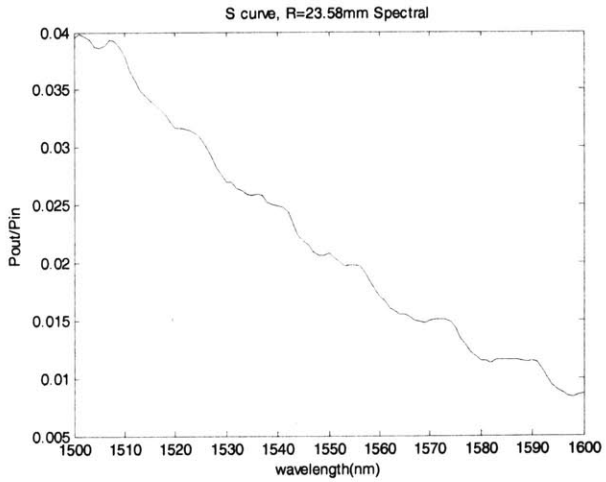

Fig. 12 Normalized transmitted power through a s-shaped bend created using two circular segments of waveguide with radius of curvature of 23.6 mm. The power after the objective was 120mW. The wavelength dependent loss causes the power to decrease by approximately 80%.

Choosing couplers with smaller radius of curvature enables the making of devices with very short interaction lengths, but the wavelength-dependent behavior of the bends makes the coupler

characteristics non-ideal. Therefore, the radius of curvature of the bends must be taken into careful consideration when designing the geometric layout of the device.

3.2.2 Geometric Layout

The coupler was designed to have straight segments connected by *s*-curves consisting of two circular pieces placed adjacent to each other. Figure 13 shows a schematic of the symmetric directional couplers. Round spot symbols mark the centers of the arcs which create the s curve. The small arrows indicate the size of the radii.

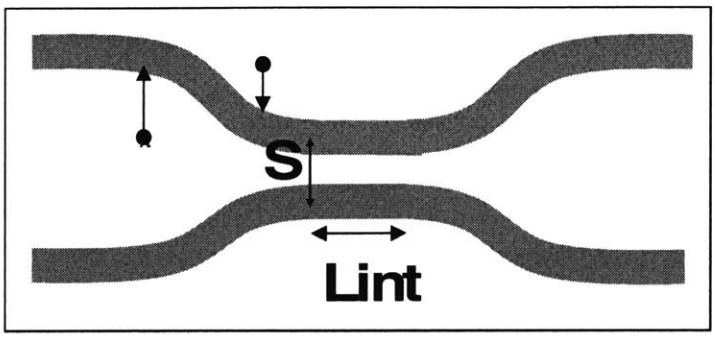

Fig. 13. Schematic showing design of symmetric directional coupler. The distance between the centers of adjacent waveguides in the interaction region S is 5um. And L_{int} was varied from 0 to 14 mm.

The interaction region separation is 5 um and the interaction length, defined by the length of the straight waveguides L_{int}, was varied from 0 to 14 mm. The radius of curvature is 86 mm. Because there can be coupling between the waveguides outside of the region of 5 um separation, the finite bend radius results in a longer interaction region than the length labeled L_{int}. As discussed above, the *s*-shaped bends also result in a wavelength-dependent loss. However, it will be shown below that with higher writing power and careful design it is possible to reduce the wavelength-dependent loss.

3.3 Spectral Results

3.3.1 Tailoring spectral characteristics

To characterize the waveguide devices, light from a tunable source from 1500 nm to 1600 nm was butt-coupled using a fiber into the ends of the polished sample. Shown in Fig. 11 are the

through and cross port coupling ratios taken from directional couplers with interaction lengths of 1mm (a) , 5 mmm(b) and 14 mm (c).

From the coupled mode equations

$$a_1(z) = a_1(0)\cos \kappa z$$
$$a_2(z) = a_1(0)\sin \kappa z$$

It can be easily seen that there is spectral dependence as the interaction length z is varied. In addition, there is variation in the parameter κz with wavelength. Since there is change in the mode size $\varepsilon_a(x)$ with wavelength, there is change in κ. From the Fig. 11, it can be seen that the coupling ratios show very little variation across the 100 nm spectrum for shorter interaction lengths and vary sinusoidally for long interaction lengths.

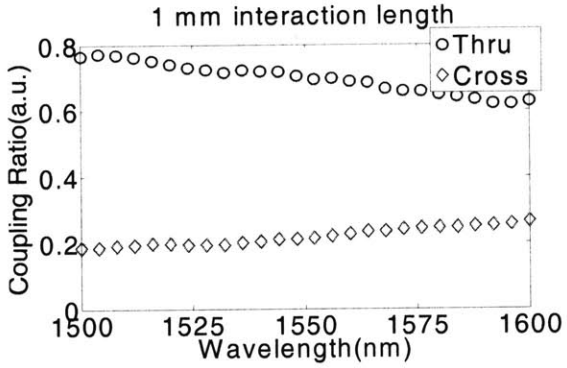

(a)

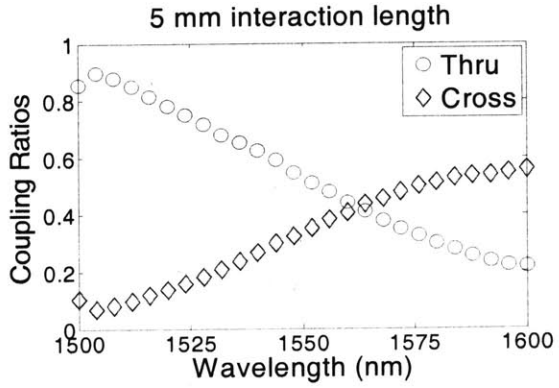

(b)

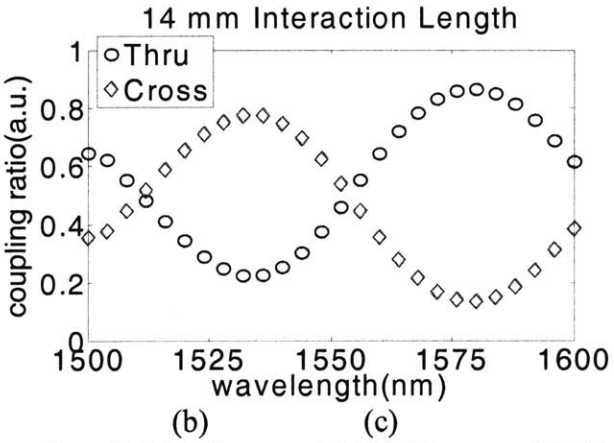

(b) (c)

Fig 11. (a) Coupling ratios with Lint =1 mm, and (b) Lint=5 mm, and (c) Lint=14 mm. Power is normalized by the losses in bent waveguides.

The data is consistent with the theory presented above. It is of note that although the amount of variation in propagation constant κ remains constant across the 100nm bandwidth, the longer interaction length shows greater variation in spectral behavior because the overall parameter κz varies more for longer interaction lengths (greater z). The variability in spectral data means shorter interaction lengths can be chosen to give wavelength independent behavior when desired, and longer interaction lengths can be used to tailor the wavelength characteristics. The contrast ratio is high, but it does not reach 1 due to a finite mismatch in propagation constants, possibly from adjacent waveguides not being identical in size or errors in z position between waveguides. This is consistent with the theoretical behavior described in equation (4) in the previous section.

3.3.2 Wavelength-independent 3dB coupler

To enable the building of more complex devices such as interferometers it is ideal to obtain couplers which act as wavelength-independent splitters. There are multiple factors which need to be taken into account toward the making of a wavelength-independent coupler. The first and most important consideration in the design is that κ, the coupling coefficient, should vary as little as possible across the desired wavelength range, which in this case is 100 nm. This can be accomplished by fabricating waveguides at higher power while ensuring single mode operation at the same time. This results in modes that are larger in size and the relative change in the mode shape in the overlap region is small. The waveguides are also placed as close together as possible without overlapping.

The second major consideration in designing wavelength-independent couplers is using the shortest possible interaction length to achieve 3dB coupling. This minimizes the value of the argument κz, meaning the device operates in the linear regime of the sinusoidal coupling dependence. This in principle is not hard to accomplish, but the effective interaction length is coupled with the choice of radius of curvature since devices with larger radii of curvature have a longer effective coupling region. In theory the length of the coupling region is well-defined. However, there is interaction between the fields in the waveguides outside of the straight waveguide region where L_{int} is defined. Thus, it is necessary to define an effective interaction length described by the total region where there is non-negligible coupling between the waveguides. Our data shows waveguides with distances of 100 um between them have negligible coupling thus 100um could be used as a cutoff distance. With larger radii, there is less wavelength dependent bending loss; however, there is increased effective coupling length. Fig. 12 illustrates the concept of two couplers having identical L_{int} but the effective interaction length is increased in the device with larger bend radii.

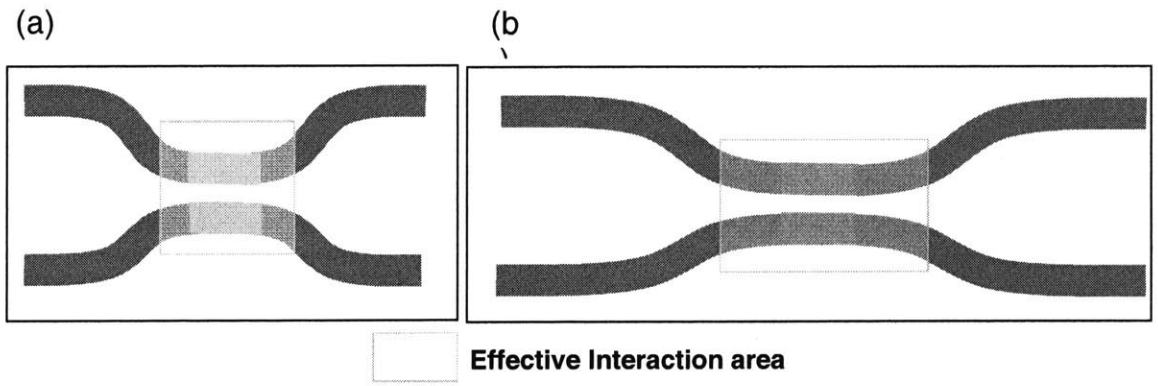

Fig 12. (a) A coupler with standard radius of curvature and L_{int}. (b) coupler with increased radius of curvature and identical Lint. The light colored box shows the region where there is non-negligible coupling. Lint is the straight portion of the interaction region(dark). It can be seen that the effective coupling length is increased when larger radii are used in the s-bend region.

To optimize the wavelength dependent loss behavior, directional couplers were fabricated with 86 mm radius of curvature and 0.15 mm L_{int}. Fig. 13 shows the wavelength-characteristics of the directional coupler.

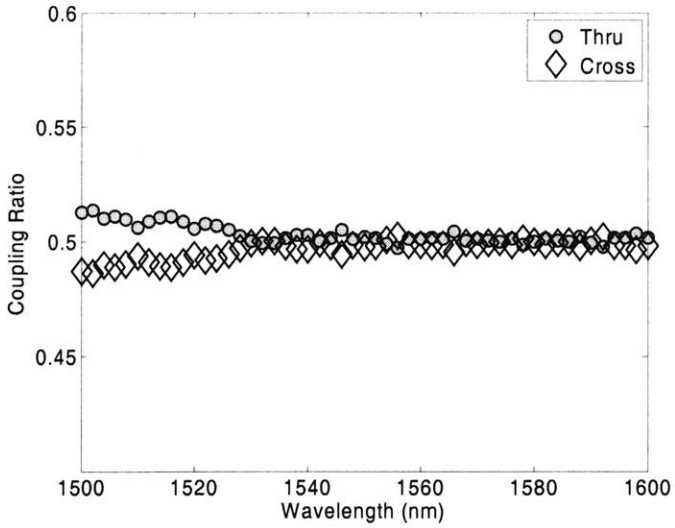

Fig 13. Spectral data for a 3dB coupler with intL= 0.15mm and 5 um interaction separation. The radius of curvature in s-bends is 86 mm. The variation in output intensities in the thru and cross ports are approximately 3%, and 6%, respectively.

The normalized coupling ratio is taken as the ratio between the thru or cross port with the sum of the powers in both ports divided by losses in a straight waveguide.Notice that although the thru and cross ports have relatively close to 1:1 coupling ratios at all wavelengths, there is still a finite variation in the absolute transmitted powers (about 3% in the thru port and 6% in the cross port) over the wavelength range 1500 nm to 1600 nm. This may be further improved by fabricating waveguides with more power to create larger modes and a less sensitive kappa parameter.

Although the coupler data shown demonstrates close to ideal behavior, it can be difficult to recreate. Since waveguide size has shown to be nonlinearly dependent on fabrication power, and the additional of components such as acousto-optic modulators to introduce loss can result in a different index contrast due to doubling of the pulse length from dispersion. Factors such as these result in variations in coupling behavior when devices are fabricated under slightly different conditions. In order to control the reproducibility of this device, it is necessary to control all writing parameters, including beam size, writing power, speed, and pulse length. With increased control and documentation, it should be possible to fabricate again a 3 dB wavelength independent coupler. The ability to create a wavelength-independent coupler enables the fabrication of more complex photonic devices, such as filters and Mach-Zehnder interferometers.

References

[1] K. Minoshima, A. M. Kowalevicz, I. Hartl, E. P. Ippen, and J. G. Fujimoto, "Photonic device fabrication in glass by use of nonlinear materials processing with a femtosecond laser oscillator," *Optics Letters*, vol. 26, pp. 1516-18, 2001.

[2] J. R. Liu, Z. Y. Zhang, S. D. Chang, C. Flueraru, and C. P. Grover, "Directly writing in fused of 1-to-N optical waveguide power splitters silica glass using a femtosecond laser," *Optics Communications*, vol. 253, pp. 315-319, 2005.

[3] T. Pertsch, U. Peschel, F. Lederer, J. Burghoff, M. Will, S. Nolte, and A. Tunnermann, "Discrete diffraction in two-dimensional arrays of coupled waveguides in silica," *Optics Letters*, vol. 29, pp. 468-470, 2004.

[4] K. Minoshima, A. M. Kowalevicz, E. P. Ippen, and J. G. Fujimoto, "Fabrication of coupled mode photonic devices in glass by nonlinear femtosecond laser materials processing," *Optics Express,* vol. 10, 2002

[5] S. M. Eaton, W. Chen, L. Zhang, H. Zhang, R. Iyer, J. S. Aitchison, and P. R. Herman, "Telecom-band directional coupler written with femtosecond fiber laser," *IEEE Photonics Technology Letters*, vol. 18, pp. 2174-6, 2006.

[6] K. Okamoto. Fundamentals of Optical Waveguides. Elsevier, Burlington. 2006.

[7] M. Heiblum, and J. H. Harris. "Analysis of Curved Optical Waveguides by Conformal Transformation." *Journal of Quantum Electronics*. Vol QE-11(2). 1975.

[8] W. Berglund, A. Gopinath. "WKB Analysis of Bend Losses in Optical Waveguides" *Journal of Lightwave Technology*. Vol 18(8). 2000.

[9] K.R. Hiremath. M. Hammer, R. Stoffer, L Prkna, and J. Ctyroky. "Analytic approach to dielectric optical bent slab waveguides." *Optical and Quantum Electronics*. Vol 37(61) 2005.

[10] J. Liu, Z. Zhang, S. Chang, C. Flueraru, and C.P. Grover. "Fabrication and optimization of one-to-two and two-to-two optical directional couplers in glass using a femtosecond laser" *Photonics North*. 2004

[11] S. M. Eaton, W. Chen, L. Zhang, H. Zhang, R. Iyer, J. S. Aitchison, and P. R. Herman, "Telecom-band directional coupler written with femtosecond fiber laser," *IEEE Photonics Technology Letters*, vol. 18, pp. 2174-6, 2006

CHAPTER 4: FEMTOSECOND LASER FABRICATION OF MACH-ZEHNDER INTERFEROMETERS

4.1 Motivation and Existing Work

4.1.1 Introduction

The demonstration of 3dB directional couplers enables the building of more complex devices. In particular, Mach-Zehnder interferometers are of interest in telecommunications, WDM, and sensing applications. The Mach-Zehnder interferometer can be used to detect properties such as non-uniform temperature and strain. A non-uniform change in temperature or strain can result in a change in the relative optical path length between the two arms, causing a change in the interference between light that has traveled the two arms. This effect can be measured either as a change in the output intensity in one arm or as a change in the period of the wavelength-dependent transfer function. Single-mode rib optical waveguide Mach-Zehnder devices in polymers have been shown to have close to 40% in intensity contrast at 980 nm in response to a non-uniform thermal radiant signal of 1.1 W in power [1]. A two-dimensional surface waveguide Mach-Zehnder device has been shown to have sinusoidal changing output as a function of applied pressure in one arm, with sensitivity of 0.053 rad/kPa at 633 nm [2]. The sensitivity of Mach-Zehnder interferometer devices also enables them to be used to characterize the change in the propagation constant of femtosecond laser scanned waveguides as functions of writing parameters such as scanning speed and exposure power.

Several groups have demonstrated the fabrication of Mach-Zehnder interferometric devices as well as their functionality. However, it has not been shown that these devices can be designed to function over larger wavelength ranges, on the order of 100 nm for example. Part of the goal of the Mach-Zehnder project was to demonstrate femtosecond laser fabricated Mach-Zehnder interferometers that function at the telecom wavelength and exhibit desirable properties such as high extinction ratio and tunability over a large wavelength range. Although there have been many studies on the index change and relative size of waveguide cross-sections of femtosecond laser fabricated waveguides, there has yet to be a comprehensive characterization of the

propagation constant. One method of measuring the propagation constant is by fabricating Mach-Zehnder interferometers with different path-length unbalances and fitting the spectral data with the known sinusoidal dependence. Thus there are two specific goals in this study: (a) demonstrate telecom range Mach-Zehnder devices which operate over a large wavelength range and (b) use the spectral characteristics of femtosecond laser written Mach-Zehnder devices to characterize the propagation constant.

4.1.2 Theory of Mach-Zehnder interferometers

Mach-Zehnder interferometers are composed of two couplers or splitter connected by optical paths of equal or unequal lengths. The theory of unbalanced Mach-Zehnder interferometers is simple and can be described using standard propagation techniques [3]. Referring to Fig. 1, the upper and lower arms are labeled A and B, respectively.

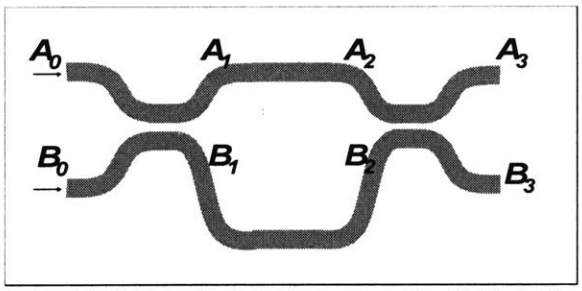

Fig. 1. Example layout of a Mach-Zehnder interferometer. The fields in the upper and lower arms are labeled A and B, respectively.

The theoretical model shown below is based on the case where light is input into the upper waveguide of the Mach-Zehnder device only, i.e. only A_0 is nonzero. The assumption is made that the waveguides constructing the two arms have identical propagation constants, such that there is no propagation mismatch parameter. For a general directional coupler, the outputs are given by

$$\begin{aligned} A_1(z) &= A_0 \cos \kappa z \\ B_1(z) &= -jA_0 \sin \kappa z \end{aligned} \tag{1}$$

For 3dB couplers, we set $\kappa z = \pi / 4$ and so that the outputs from the first coupler are:

$$\begin{aligned} A_1 &= \frac{A_0}{\sqrt{2}} \\ B_1 &= -j\frac{A_0}{\sqrt{2}} \end{aligned} \tag{2}$$

(2)

Propagation through two unequal distances or optical path lengths can be represented by an identical phase shift βL and an additional phase shift ϕ experienced by only one arm. After passing through the straight portions of the upper and lower arms, the fields have different phase shifts and can be represented as

$$A_2 = A_1 \exp(-j\beta L) = \frac{A_0}{\sqrt{2}} \exp(-j\beta L)$$
$$B_2 = B_1 \exp(-j\beta L + j\phi) = -j\frac{A_0}{\sqrt{2}} \exp(-j\beta L + j\phi) \tag{3}$$

These two fields are then input into the second directional coupler, which is also assumed to be a 3-dB coupler, and the total resulting fields in the two arms can be represented by two sinusoidal functions with the difference in phase shift split between them:

$$A_3 = -jA_0 \sin\left(\frac{\varphi}{2}\right) \exp\left(-j\beta L + j\frac{\varphi}{2}\right)$$
$$B_3 = -jA_0 \cos\left(\frac{\varphi}{2}\right) \exp\left(-j\beta L + j\frac{\varphi}{2}\right) \tag{3}$$

The optical intensity is given as the absolute value of the field square and oscillates sinusoidally as a function of the phase difference as shown below

$$|A_3|^2 = |A_0|^2 \sin^2\left(\frac{\varphi}{2}\right)$$
$$|B_3|^2 = |A_0|^2 \cos^2\left(\frac{\varphi}{2}\right) \tag{4}$$

With change in wavelength, this oscillation is expected to be seen as a result of the variation of φ experienced by difference wavelengths. The period of the oscillation is determined by the value of the unbalance. Note that when there is no unbalance, ϕ is zero and the transfer function of the upper arm is unity for all wavelengths. Due to time reversal symmetry, there is a change in the contrast ratio of the Mach-Zehnder if the couplers are not perfectly 3dB [4]. However the positions of the nulls do not change.

4.1.3 Existing Mach-Zehnder Device Fabrication

An earlier femtosecond laser fabricated Mach-Zehnder interferometer consisted of two back to back X-couplers [5]. The crossing angle was optimized at 2 degrees. The path length difference was designed to be 10 μm. A schematic of the device and a phase contrast microscope image of the crossing region are shown in Fig 2.

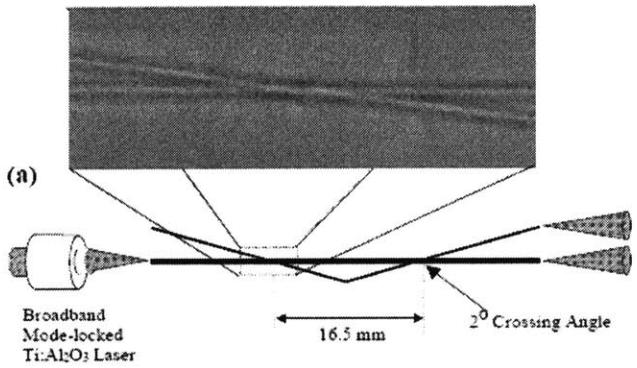

Fig 2 from ref [5]. Layout of the unbalanced Mach-Zehnder consisting of two X couplers. And contrast microscope image of the crossing region.

The total length of the devices is 16.5 mm. The path length difference between the two arms was approximately 10 μm. Light was coupled into the interferometer and split into the two arms at the first X-coupler, traveled different path lengths, and underwent constructive or destructive interference at the second X-coupler, depending on the wavelength. Because the optical path length changes with wavelength, the unbalanced path length Mach-Zehnder interferometer can function as a wavelength dependent filter. The wavelength dependent behavior of this device was measured using a broad-band, mode-locked Ti:sapphire laser centered at 800 nm. The transfer function, normalized with respect to the input spectrum, shows clear interferometric fringes, as reproduced in Fig. 3 from ref [5].

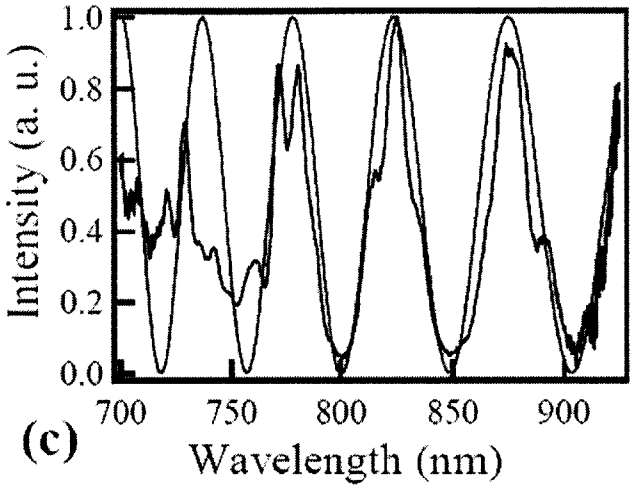

Fig 3 from ref [5]. The normalized output intensity spectrum of the X-coupler Mach-Zehnder device. The smooth curve is the theoretical curve of the device with path length difference of 9.3 μm.

The interferometric fringes can be clearly observed in the normalized output spectral data and demonstrates the expected wavelength filtering behavior of an unbalanced MZ interferometric device. Notice that there is reduced oscillation at shorter wavelengths which may be due to the larger fluctuations of the input light spectrum or to the possible onset of higher order modes. The smooth curve shows the theoretical wavelength dependence of the transfer function for the path length difference of 9.3 μm, and it can be seen that the experimental measurements are in close agreement with theory. The difference between theoretical path length of 10 um and measured path length of 9.3 um is 0.7 um out of 16.5 mm, or on the order of 10^{-5}. This error is most likely due to small errors in the translation of the translation stage, which results in differences in the refractive index between the waveguides in the two arms of the device. As can be seen in the following data, significant improvements have been made in the fabrication of different path length MZ interferometers. Since this particular device was the first demonstration of the fabrication of a MZ interferometric device using femtosecond laser writing, and from the spectral data, it can be seen that there are improvements to be made in the accuracy of the output behavior at lower wavelengths as well as in the smoothness of the spectral data.

In 2003, Florea et al. demonstrated the fabrication and characterization of a more advanced MZ optical interferometer [6]. The device was provided by Translume, Inc., Ann Arbor, MI. A schematic diagram of the devices is shown in Fig 5 from ref [6].

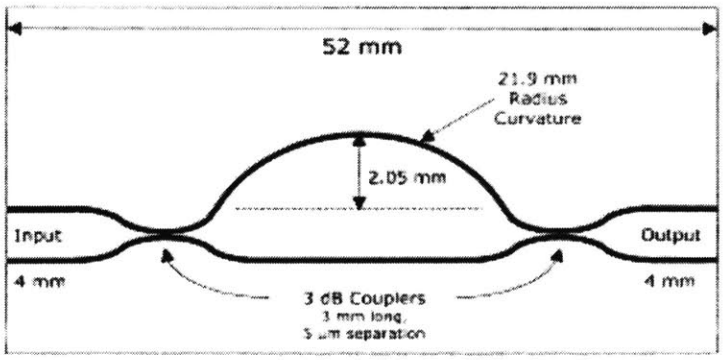

Fig 5 from ref [6]. A Mach-Zehnder interferometer composed of two directional couplers. This device has the advantage of avoiding excess losses from sharp waveguide bends.

The device is an unequal path-length MZ interferometer consisting of two 3dB directional couplers. This design has no sharp bends and is made entirely from curved waveguides. The path-length difference between the two arms is approximately 0.6 mm, corresponding to a spacing between adjacent maxima of 0.7 nm at a wavelength of 778 nm. The MZ device was characterized using a broadband source centered around 776 nm, and the output spectrum was taken from 776 nm to 780 nm. The spectral characteristics are shown in Fig. 6.

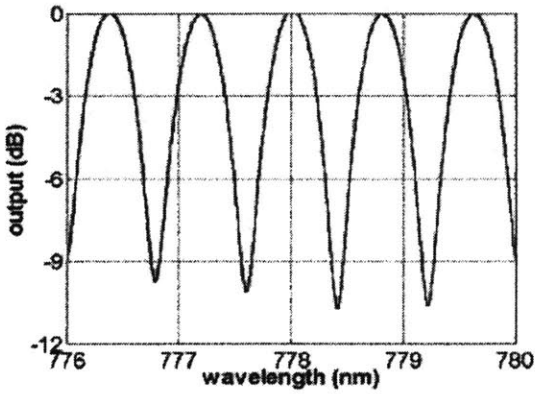

Fig 6 from ref [6]. Spectral characteristics of the coupler-based Mach-Zehnder interferometer. The data shows relatively high extinction ratio over a wavelength range of 4 nm

The output spectrum was taken from a single arm, and the channel spacing can be observed to be approximately 0.75 nm. The channel spacing is 0.05 nm, off from the expected value of 0.7nm, and the spectral data appears to be smooth. The extinction ratio is as high as around 10 dB. The advantage of this device is that it eliminates losses due to sharp bends in the waveguides which were present in the previous paper, and replaced X-couplers with directional couplers. However, the data shown is only over a very small wavelength range of 4 nm and the independent spectral data of the directional couplers is not shown. Therefore, it cannot be determined whether the

directional couplers display wavelength independent behavior over a large range of wavelengths. Furthermore, since most telecommunications wavelengths center around 1550 nm, it is useful to demonstrate such a device at the telecom wavelength.

Mach-Zehnder Interferometers have applications in sensing changes in external parameters in one arm and are also used in telecommunication networks to separate or combine signals. The ability to fabricate such devices with good repeatability requires being able to control the path length difference between the two arms with a high level of precision. It is also important to understand how to tune Mach Zehnder devices to achieve the desired wavelength response. Recently, it has been shown that devices such as interferometers can be tuned after initial fabrication to achieve desirable characteristics, a process called "trimming" [6,7]. "Trimming" is the process of tuning existing device characteristics through additional laser exposure. With the assumption that index of refraction can be modified cumulatively, additional laser exposure creates longer optical paths by making additional changes to the index. Trimming can be used to improve the contrast ratio of Mach-Zehnder devices by optimizing couplers for 3dB operation. It has been shown that trimming can be used to change the waveguide's cross-section, giving the ability to correct polarization-dependent behavior. As shown in Fig. 6 from ref [6], trimming is also used to tune the optical path difference between two arms of a Mach-Zehnder device, thereby changing the phase of the periodic spectral behavior.

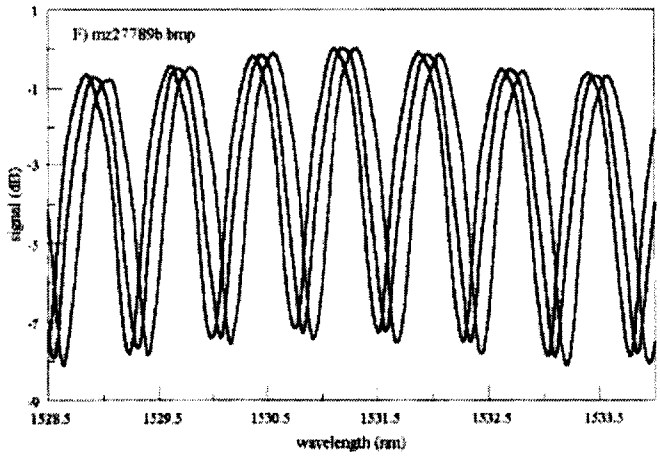

Fig.6 from ref [6] Demonstration of shift in spectral shift with successive "trimming" of the optical path in one arm of a Mach-Zehnder device.

One arm of the device is exposed to additional femtosecond laser pulses while the changes in spectral behavior are monitored in real time. It can be seen that the device's spectral response, namely the position of the minima and maxima, is tuned by additional femtosecond laser exposure. This data is impressive since it shows the well-controlled shifting the maxima positions of the Mach-Zehnder device as one arm is exposed to additional femtosecond light. However, the range of tuning shown is very small, only a fraction of a nanometer, and once, again the device is shown to operate only over a small wavelength range of 5 nm.

Questions can be raised as to whether trimming has limitations since increased exposure is expected to eventually lead to changes in the waveguide size and profile, opening the possibility of the change of a single-mode waveguide to multi-mode operation, as well as the addition of increased loss due to mode mismatch between existing waveguides and the waveguide region which has been trimmed. It is possible that the "trimming" technique cannot be used to change the wavelength characteristics of a MZ device by more than a nanometer or so due to these limitations and therefore is difficult to use in correcting the behavior of devices which have an error in wavelength characteristics of more than a nanometer. It has also not been shown whether the "trimming" technique is repeatable, although it appears to be well-controlled. It is necessary to show that for two different devices fabricated at identical powers, trimming shifts the position of the maxima by the same amounts or within an accepted error range. As such "trimming" is impressive because it seems to preserve the high contrast ratio and exactness of the spacing between maxima of the MZ device in the data which is shown, but it seems to be limited since it can only be used to shift the wavelength characteristics of the device by less than a nanometer and may cause additional losses due to modal mismatch.

4.1.4 Mach-Zehnder interferometer applications

As described earlier, Mach-Zehnder interferometers are extremely sensitive to changes in the propagation constant and therefore can be used in sensing applications in terms of change in mechanical strain, pressure, temperature, or other parameters. In 2005, Yang et al. reported on the fabrication of MZ interferometers in a temperature sensing application [8]. Mach-Zehnder interferometers were fabricated in amorphous silica using a femtosecond laser source at 800 nm and a repetition rate of 1kHz. After the demonstration of Y couplers and directional couplers, an

equal-length Mach-Zehnder interferometer was fabricated. This Mach-Zehnder interferometer has a simpler design since it consists of two Y splitters connected by straight waveguides. Notice that Y splitters are simpler devices than directional couplers. However, they are generally wavelength-independent and are easier to design and fabricate. The Mach-Zehnder interferometer fabricated here was completely balanced with no path-length difference, and is therefore expected to have no wavelength-dependent behavior.

Fig 7 from ref [8] shows a schematic of the laser direct written MZ devices and the change in output intensity as a function of time while one arm of the interferometer was heated by a soldering iron.

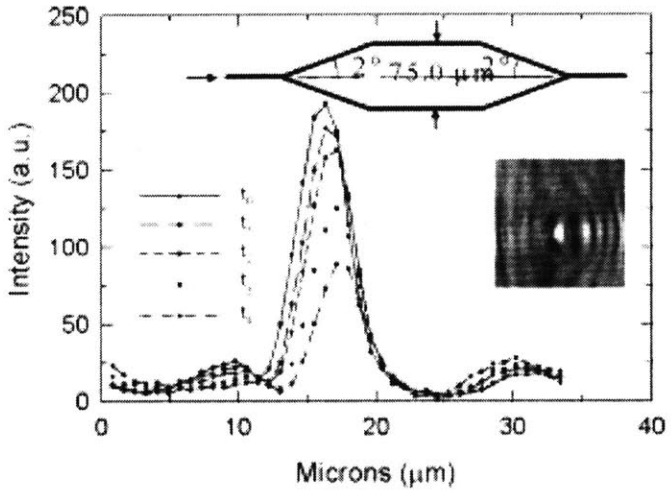

Fig 7 from ref [8]. Schematic of MZ device consisting of two Y-splitters and time response of output intensity as heat is applied. Time increases from t_0 to t_4.

It is not defined what the temperature of the soldering iron was, and the paper does not contain a discussion of the thermal properties of the glass and its expected response to a point heat source. It is assumed that the soldering iron produces local heating which changes the refractive index of the waveguide and creates a phase shift between two arms. This is what the authors speculate alters the intensity of the interference pattern. As the glass temperature near the soldering iron progressively increases, the amount of phase shift is presumed to increase and the overall output intensity due to interference from both arms is observed to decrease. This result is one of the first demonstrations of the application of femtosecond laser direct write Mach-Zehnder devices to sensing applications.

The time evolution of the intensity seems to support progressive heating of the material over time. It would be desirable to show the absolute scale of time that has passed and to demonstrate that this is consistent with the known heating properties of amorphous silica. In addition, it is desirable to show the wavelength characteristics of the MZ device and demonstrate a shift of the waveguide characteristics. If the normalized intensity of the balanced device is unity, it is necessary to see the behavior of the wavelength characteristics over time to determine the direction of the shift, which can indicate the direction of motion of the maxima. This would show whether the effective optical path length has increased or decreased. Moreover, the soldering iron is assumed to have an effect on the refractive index of the waveguide, but it is possible that the effect of the heating on the refractive index of the waveguide is minor, and that the main effect of the heating is to cause the substrate to expand non-uniformly. Non-uniform expansion of the substrate between the two arms of the devices can also produce a change in the output intensity as it can create a path-length difference between the two arms. It is not stated where exactly the heating source was placed, and it is difficult to understand the dimensions of the devices from the figure that is shown. However, a difference of a millimeter from a point source can produce a significant difference in expansion, resulting in a detectable difference in path-length. The coefficient of thermal expansion of a typical fused silica sample is 0.5 ppm/°K.

In summary of this section, Yang et al. have demonstrated a unique measurement of the feasibility of the use of femtosecond laser direct write MZ devices for temperature sensing. It is difficult to gauge the accuracy of the measurement since the temperature of the heat source is unknown, and it cannot be seen from the data whether the shift in the maxima is toward the right or the left. In addition, it is not proven or argued that the heat source creates a change in refractive index of the waveguides instead of creating a path-length unbalance due to thermal expansion.

An additional application of MZ devices is in electro-optic modulation configurations. By applying a voltage across one arm of a balanced device, it is possible to use the electro-properties of the glass and change the phase shift between the two arms to π by applying the correct voltage. The intensity output of the device can be switched between zero and unity before by switching the applied voltage on and off. Because of the low electro-optic response of fused silica, there has yet to be a successful MZ electro-optic modulator displaying full unity to zero switching.

However, it has been shown that the use of thermal poling on one arm of a laser fabricated Mach-Zehnder can tune the spectral response via the electro-optic (EO) effect [9]. Based on spectral shift from a voltage applied across one arm of a femtosecond written MZI, the EO coefficient of Herasil fused silica was estimated to be 0.17 pm/V. As shown in Fig. 8 from ref [9], an average spectral shift of 1 nm in the output spectrum can be obtained by applying a voltage of 400 V transversely across one arm of the unbalanced MZ interferometer.

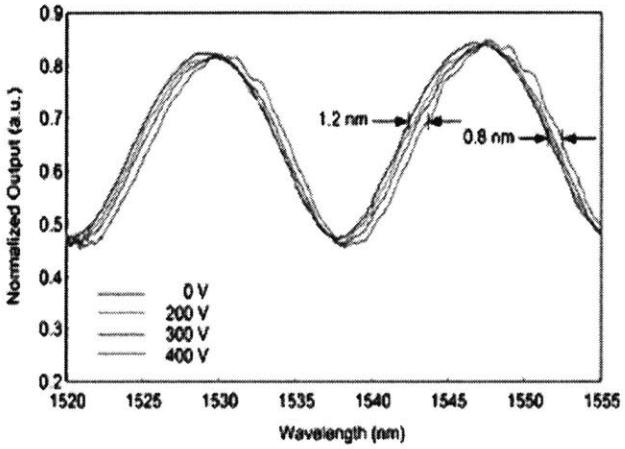

Fig 9 from ref [9]. An in crease in spectral shift in the output of a femtosecond laser fabricated MZ device as voltage is applied across one arm.

Based on this measurement, the authors expect that a voltage of 1000V may be able to create a complete switch between on and off stages if the length of the electrodes are increased, and the depth and input polarization are optimized. Although the integrated MZ interferometric Electro-optic modulator currently demonstrated does not perform as well as conventional EO materials, such as lithium niobate, the demonstration of this technique has significant implications.

In addition to different types of fused silica, MZ devices have also been fabricated in crystalline structures. In 2006, Mendez et al. presented the fabrication and characterization of femtosecond laser direct-write MZ interferometers in Lithium Niobate [10]. Lithium Niobate is an important material because of its excellent non lineal, acousto-optics properties, and is one of the most important substrates used for optoelectronics devices. Femtosecond laser direct write in these materials opens the possibility of fabricating embedded waveguides at low cost and with one step. As in other substrates, it is necessary to consider losses caused by bending or curving of the waveguide, and the first study was to optimize Y splitters which contain acceptable bends. The bending angle was varied by changing the separation between the arms of the MZ device from

12 um to 30 um, and propagation loss was measurement at different bending angles. The loss as a function of the bending angle was shown to varying between 1 dB/cm at 0.16° and 7 dB/cm at 0.39°. Once the issue of bending is addressed, a simple MZ interferometer was designed. Fig 10 from ref [10] shows the femtosecond laser direct write MZ schematic.

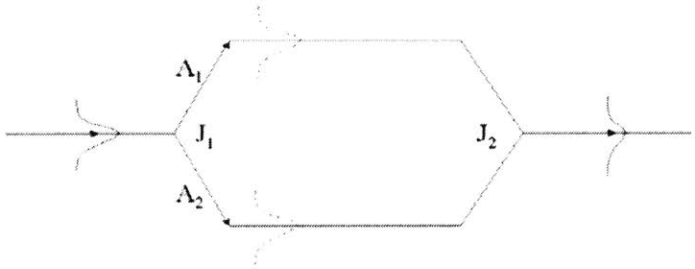

Fig 10 from ref [10] Schematic of balanced MZ interferometer fabricated in Lithium Niobate crystal.
The length of the arms is 5 mm.

Once again, the design is quite simple since the device consists of two Y splitters and two straight waveguide regions. The transmitted intensity should be nearly unity since the arm lengths are balanced. The arm lengths of the MZ interferometer were set to be 5 mm. Fabrication was performed on commercially obtained z-cut Lithium Niobate crystal using 120 fs laser pulses from a 1 kHz repetition rate Ti:Sapphire laser up to 1 mJ of energy. Translation velocity was set at 25 um/s which give the most efficient channel waveguides supporting a well-confined single mode. Fig 11 from ref [10] shows the optical microscope photograph of Y junctions which were used to create the MZ device. The size of the single-mode waveguide is around 6-7 um.

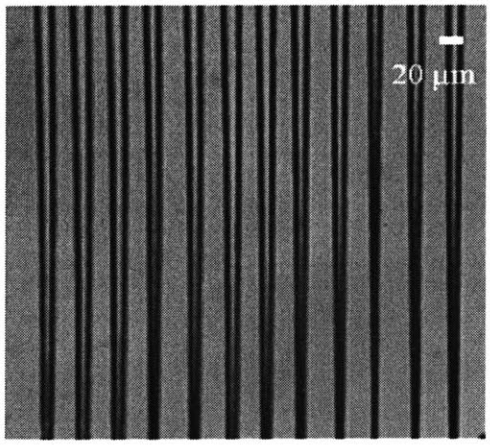

Fig. 11 from ref [10] Microscope photograph of Y junctions written in Lithium Niobate.

After waveguide input and output facets are polished, light from a He-Ne laser at 632.6 nm was coupled into the input end using a 10x microscope objective. The coupling efficiency was reported to be 5%. The output was focused using a 10x objective and imaged onto a CCD camera to record the modal profile. Fig. 12 from ref [10] shows the CCD image of the output profile of the He-Ne beam after passing through the MZ interferometer.

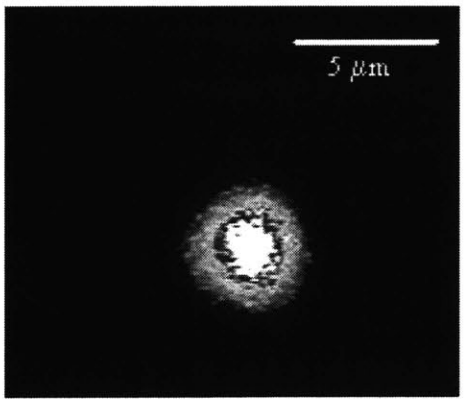

Fig. 12 from ref [10] CCD camera image of the output intensity profile in MZ device fabricated in Lithium Niobate. Single-mode operation was confirmed at both 808 nm and 1550 nm.

From the modal output it was verified that both TE and TM polarizations are single mode and have similar propagation characteristics. Single mode guiding was also observed at the two different wavelengths of 808 nm and 1550 nm. In summary, this work demonstrated the femtosecond laser direct-write of a balanced Mach-Zehnder interferometer in crystalline Lithium Niobate. The work is the first known demonstration of the fabrication of an MZ device in a crystalline material and opens the door to more complex devices. The loss is systematically characterized as a function of bending angle and a reasonable loss is shown to be possible if the bending angle is sufficiently small. Future work on this project should entail, once again, a more complete characterization of the devices, including a measurement of the spectral characteristics. It is useful to verify that the device is indeed balanced by showing the wavelength characteristics do not vary. It would also be important to observe the repeatability of structures in crystalline materials and to investigate the mechanism of index modification since it can be expected to be different from the mechanism of index modification in amorphous silica.

As can be seen, Mach-Zehnder devices can be used as temperature sensors, electro-optic switches, or wavelength filters, and some of these applications have already been demonstrated

in femtosecond laser written devices in glass. Future work involves expanding the functionality of femtosecond laser fabricated MZ devices and applying them in more complex photonic networks.

4.2 Unbalanced Mach-Zehnder Interferometers at Uniform Speed

4.2.1 Design of Unbalanced Mach-Zehnder Interferometer

To accomplish the goal of demonstrating a femtosecond laser written Mach-Zehnder device with over 100 nm wavelength range, it is necessary to consider carefully the geometric design. The ideal Mach-Zehnder interferometer design consists of two 3 dB wavelength-independent couplers connected by smooth curves to two unbalanced arms. It is desirable for the couplers to have no wavelength dependence because this enables measurements to depend solely upon the characteristics of the two arms. In practice, it is possible to fabricate directional couplers which are close to having the ideal behavior, but because of limitations such as wavelength-dependent loss and finite waveguide size, there can be some deviations. These factors were discussed in the previous chapter.

It is important to note that when there is non-ideal splitting ratio, i.e. the splitting ratio is not 1 to 1, the contrast ratio is decreased because the maxima of the peaks do not reach unity, but the intensity at the nulls remains zero. Because of the principle of reversibility [4], the position of the nulls does not change with non-ideal coupler splitting ratio. This can be explained in Fig 13 below reprinted from ref [4].

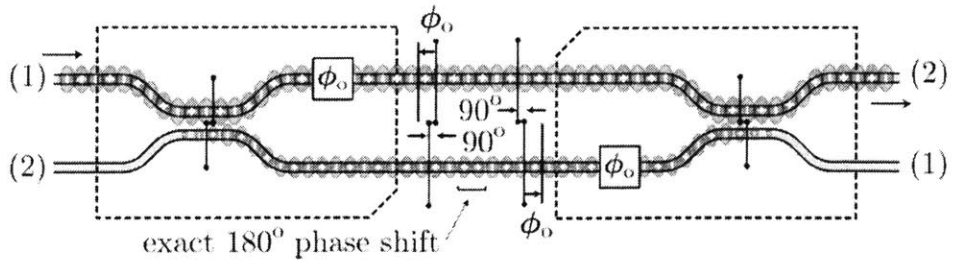

Fig 13 from ref [4]. A null can be thought of as 90° phase shift experienced by the forward propagating wave, in the first half of the MZ. If the second half of the device is symmetric, the wave can be thought of as time-reversed. This results in a null in the second arm independent of coupler characteristics.

After the coupler, the wave experiences some propagation. If the propagation is identical between the two arms and the second coupler is identical with the first, the forward propagating wave through the second coupler is equivalent to a backward propagating wave through the first coupler. This is equivalent to time-reversal. In this case, the wave experiences destructive interference regardless of coupling ratio. Thus, the positions of the nulls do not change when there is non-ideal coupling ratios, and any measurements which depend solely upon the positions of the minima, are unaffected.

From the figures in chapter 3, it can be seen that a coupler with L_{int} parameter of 1 mm has very small amount of wavelength dependence (about 12 %). The couplers used in the design of the Mach-Zehnder devices to be presented have L_{int} set at 0.15mm to optimize for 3dB operation. They have less than 5% variation in output intensity across the wavelength of 1500 to 1600 nm and an even smaller variation in coupling ratio. Fig 14 shows a schematic of the Mach-Zehnder interferometer. S bends were fabricated by placing two circular pieces of waveguide next to each other at the point of tangency.

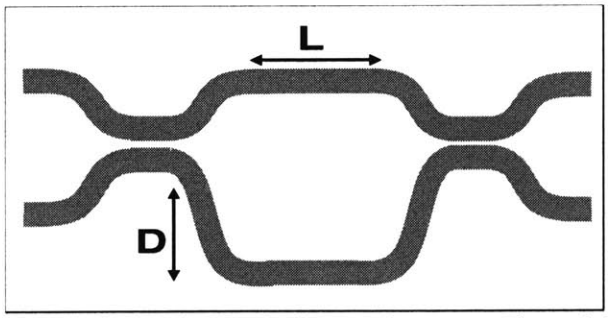

Fig 14. Schematic of unbalanced Mach-Zehnder interferometer. The path length unbalance is changed by changing the vertical dimension D.

The wavelength dependence of the bends in the structure is a factor in Mach-Zehnder design just as it was a major factor in coupler design. To minimize wavelength dependence, the longer arm has bend radius of around 300mm. To create the desired sinusoidal periods in the 1500 nm to 1600 nm range, it was necessary to use smaller bend radii on the longer arm. The radii are varied between 100 and 233 mm. The unbalance was adjusted by changing the vertical dimension of the S bend on the lower arm and varied between 10um to 100um. There are alternative ways to alter the unbalance. This design has the advantage of being compact and easy to alter. However, it has the disadvantage of different bending losses between the arms. The Mach-Zehnder device was designed for two purposes: to measure the absolute value of the

propagation constant by observing the period of the wavelength dependence for different unbalances and to find the variation of propagation constant with writing parameters such as speed and power. As will be shown in the next section, the current design for the Mach-Zehnder device is sufficient to achieve the goals mentioned above. For the next set of devices, however, many improvements can be made.

4.2.2 Spectral results

Spectral results for Mach-Zehnder devices of path length differences 17.8 to 100.6 um are shown in Fig 15 (a) and (b). Data is normalized with respect to losses in a straight waveguide. Note that wavelength-dependent bending losses are present.

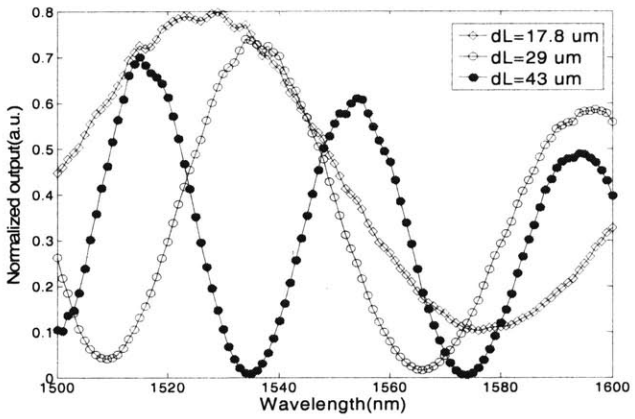

(a)

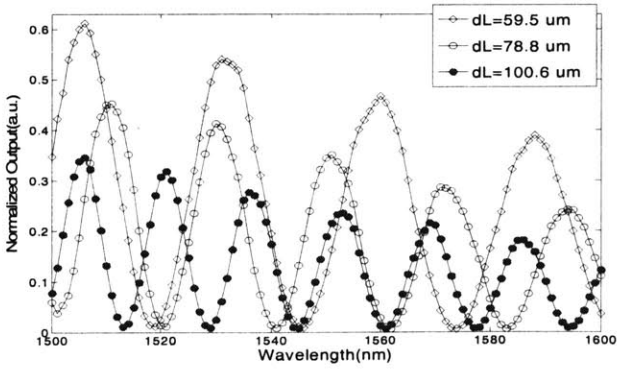

(b)

Fig 15 from ref [11] spectral characteristics of MZ interferometers with path length differences of (a) 17.8-43 um and (b) 59.5-100.6 um. As expected, oscillation period decreases with increasing path length.

As expected, the period increases for larger path length differences and decreases for shorter path length differences. This means the characteristics of the device can be tailored by changing the path-length unbalance. The contrast ratio decreases as a function of wavelength. This is most likely a result of the wavelength-dependence of the bending loss. To support this, it is clear that the roll-off in wavelength of the coupling ratio is more pronounced for devices with larger unbalance, or sharper bend radii. The MZ data shows high contrast ratio, with nulls approaching nearly 0 for all devices. As discussed earlier, the contrast ratio is controlled by the splitting ratio in the two couplers which compose the MZ interferometer. However, the magnitude of the coupling ratio at the nulls is unaffected, as are the positions of the nulls in the spectral behavior of the device.

With a sinusoidal fit for the wavelength characteristics of each Mach-Zehnder device, it is possible to calculate the absolute value of the propagation constant by noting that the variable inside the sine squared argument in Equation (4) φ, is equal to the product of the path length difference and the propagation constant. Therefore, once φ is known for a particular wavelength, finding the propagation is quite simple:

$$\frac{\varphi(\lambda)}{2} = \frac{\beta(\lambda)L}{2}, \qquad \beta(\lambda) = \varphi(\lambda)/L \tag{6}$$

For each measured set of spectral data with dL from 17.8 um to 100.6 um, a theoretical fit for the theoretical behavior was performed, and the value of the propagation constant β at 1550 nm was calculated from the argument φ . There is some variation in this propagation calculation for data obtained from different devices, but the value is consistent to within 2%. Using the above information, the absolute value of the propagation constant at 1550 nm for waveguides fabricated at 12 mm/s and 120 mW exposure is approximately $\beta = 5.8x10^6 \pm 0.1x10^6$. Notice that the air-bearing stage has errors on the order of 10 nm in position and around 0.001 mm/s error in fabrication velocity. The propagation constant is estimated based on the assumption that the path-length unbalance is correct to the theoretical value. More importantly, fluctuations in laser output power were as high as 5% and can cause variations in β along the waveguides, while the

proposed calculation assumes β to be constant. Thus, the calculation for the propagation constant has some sources of error, but between six different devices the variation in the calculation is small.

In summary, the above data shows that Mach-Zehnder interferometric devices can be fabricated using the novel MPC laser system, and that the spectral characteristics can be controlled by controlling the path-length unbalance. Furthermore, fabricating Mach-Zehnder devices at different path-length unbalances and fitting the spectral data is a method for measuring the propagation constant of femtosecond laser fabricated waveguide devices. Multiple devices with different path length unbalances allows for multiple data points to be compared against each other. However, the calculation must assume the path length unbalance dL is known to within a good accuracy. It is also affected by fluctuations in laser power which change the size and index of the waveguide in a nonlinear fashion. There is some variation expected between data taken from identical devices, and a necessary future step is to make multiple measurements for each unbalance length.

4.3 Characterization of Propagation Constant Dependence on Writing Speed

4.3.1 Motivation

It is important to not only understand the propagation constant at the initial writing conditions, but also how it changes in response to varying exposure conditions. To this end, one can exploit the Mach-Zehnder interferometer's sensitivity to propagation constant. As mentioned earlier, Mach-Zehnder devices have been used in various sensing applications including temperature, strain, pressure, and chemical sensing. If there is a small change in propagation constant in one arm, there is a shift both in the phase and period of the spectral behavior in both the thru and cross port intensities. The goal for the second set of proposed studies with MZ interferometers was to observe the change in propagation constant with respect to changes in writing conditions, namely scan speed and exposure power.

For a small change in propagation constant in one arm, the first order effect on the fringes is a linear shift, or a phase change. The first proposed experiment was to characterize the change in propagation constant as a function of writing speed. It is important to realize that it is difficult to decouple writing parameters on waveguide size and index change, since doing so requires the ability to alter only the waveguide size or index change, while changing the scanning speed, for instance, can alter both. However the measurement of the propagation constant is a way to characterize the combined effect of index change and waveguide size, since the propagation constant is a result of the solution of the waveguide equation, which is dependent on both the size and index of the waveguide. For a small change in propagation constant, there is a shift in the positions of the nulls in the MZ spectra. Changes in propagation constant could be calculated from the observed shifts in the nulls and maxima of the spectral data.

4.3.2 Mach-Zehnder experimental design

Fig 17 shows the schematic of the Mach-Zehnder device which was designed for measuring changes in propagation constant.

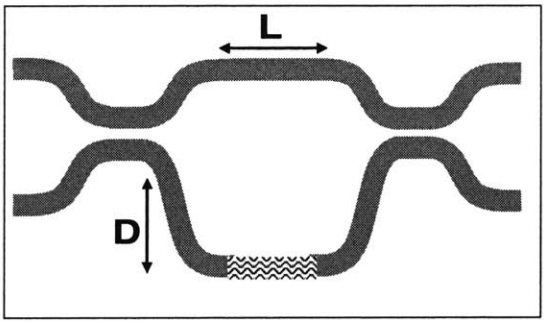

Fig 17. Schematic of Mach-Zehnder device designed to measure changes in propagation constant. The straight portion of the second arm(patterned) is written with a different speed.

The design of the device is quite simple: a Mach-Zehnder with the identical design as the device in section 4.2 is written with a different speed (speed2) in the straight portion of the bottom arm, which has a length of 2 mm. The change in propagation constant in this perturbed waveguide is expected to result in a change in the spectral data of the thru port intensity when measured using a tunable source across 1500 nm to 1600 nm.

The straight waveguides written at speed2 will be analyzed to ensure that they are still single-mode. A smooth velocity transition will be made using the air-bearing stage to connect the sections written at 12mm/s and sections written at speed2. A change in scanning speed is expected to produce a change in propagation constant, which can be observed in a phase shift of the periodic spectral pattern. For small changes in propagation constant, the period of the spectral pattern is expected to remain close to its original value. Thus, the only change is expected to be a shift in the positions of the nulls.

4.3.3 Spectral Results

Fig. 18 shows the spectral features of a set of Mach-Zehnder devices written with four different speeds in the extended arm.

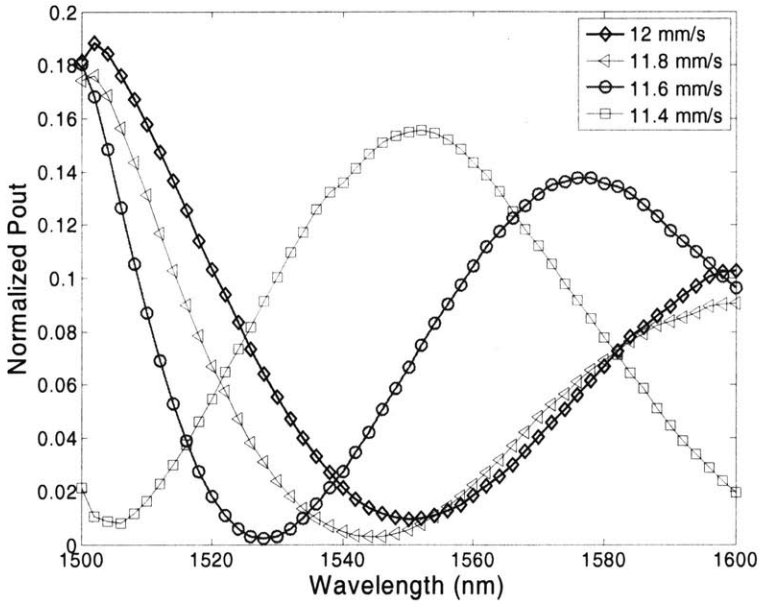

Fig 18. Normalized spectral output for Mach-Zehnder with identical path length differences and speed2 of 12 mm/s to 11.6 mm/s

Because there was some variability in the data between identical devices, each Mach-Zehnder device with a different speed2 parameter was fabricated four times, and the figure shows the median data sets. As expected, a change in scanning speed produces a change in propagation constant, which can be observed in a phase shift of the periodic spectral pattern. To estimate the change in propagation constant, the position of the minima was measured and the change in β is

calculated from equation (6) above. Table 1 shows the estimated changes in propagation constant at 1550 nm as a function of the writing speed in the second arm. For reference, the propagation constant change is set to be zero for the device with speed2=12 mm/s, and other propagation constants are shown as a change with respect to the reference point. Because multiple sets of data were data, each point has a variance as shown.

Speed2 (mm/s)	Minima position (nm)	$\partial\beta$
12	1550	0
11.8	1544	$3.3\text{x}10^4 \pm 1\text{x}10^4$
11.6	1528	$6.3\text{x}10^4 \pm 2.4\text{x}10^4$
11.4	1506	$9.7\text{x}10^4 \pm 1.5\text{x}10^4$

Table 1. Estimated changes in propagation constant calculated from Mach-Zehnder devices with changed writing speed in one arm.

From the results shown, it can be seen that the spectral pattern appears to be very sensitive to fabrication conditions. The change in propagation constant seems to increase monotonically with larger differences in speed. The data points for $\partial\beta$ lie outside each other's error ranges, indicating statically significant changes in propagation constant as a function of writing speed. However, it must be noted that between four identical devices there was variation in the spectral data. Errors in stage velocity can produce a small amount of uncertainty in the measurement, but waveguide properties are nonlinearly dependent on writing power, so a larger part of the error in this measurement was expected to be a result of fluctuations in laser power. The measurement of the phase shift of the Mach-Zehnder intensity output in the spectral domain is an important technique for characterizing changes in waveguide properties as a function of writing condition.

4.3.4 Improving repeatability

One significant issue in making the measurement of change in propagation constant with writing speed is the repeatability of identical devices. To make a statistically significant calculation in the change of propagation constant with writing speed, the variance in the maxima and minima positions of the spectral characteristics of MZ devices with identical structures must be small enough to provide a reliable comparison between MZ devices with different speed2. In other

words, the variance in a particular set of identical MZ devices must be small compared to the average minima positions of different sets of MZ devices.

As mentioned above, errors in stage position and writing speed play a relatively small role in the error of the measurement. However, waveguide properties are heavily dependent upon the writing power. Since the laser power could fluctuate up to 5mW at 180mW writing power, there was significant variation between devices which were meant to be identical. To control this error, the laser must be operated at the optimal position, and a feed forward power control scheme was implemented by Dr. Josh Chung using a three-parameter computer program and an Acousto-Optic Modulator (AOM). Labview was used as the machine-AOM interface. Fig 19 from ref [12] shows the schematic of the power control setup.

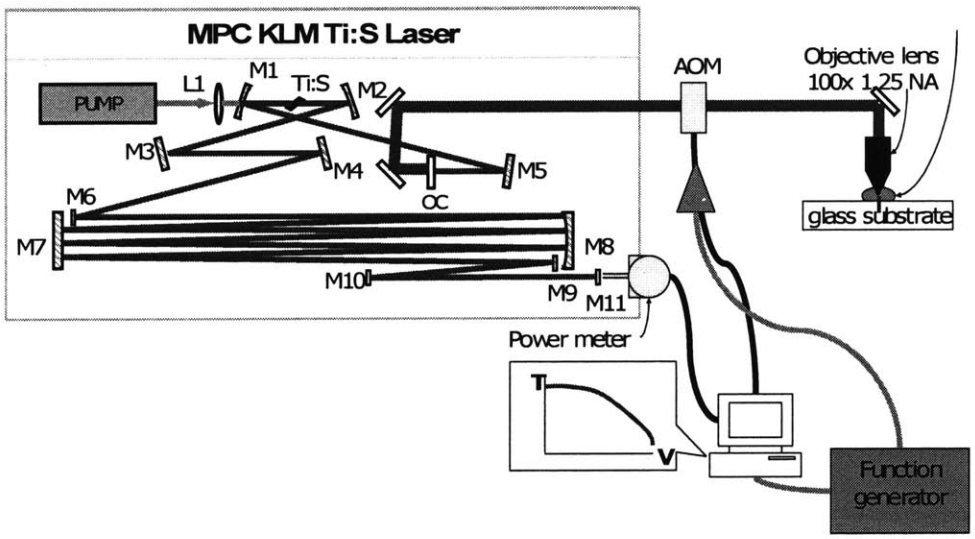

Fig 19 from ref [12]. Schematic of power-controlled laser power stabilization scheme using an AOM.

A small fraction of the power is split off using a polarization-sensitive beam splitter and measured using a fast germanium detector. The output power is fed into the computer via a GPIB card. The Labview program interfaces with the GPIB board, then outputs an appropriate value to a DAQ board which controls the AOM. The output voltage controls the AOM to create enough loss in the beam to stabilize the power.

The power fluctuation before the implementation of the AOM feed-forward scheme was 5mW over 15 seconds. The laser power fluctuation after implementing the power control scheme was

2 mW over time scales of 15 seconds. Fig. 20 shows an example of improved repeatability measurements. Before implementation of power stability, repeatability of null positions was on the order of 10-15 nm. With power control and proper stage tuning, repeatability of null positions can be as good as a few nanometers.

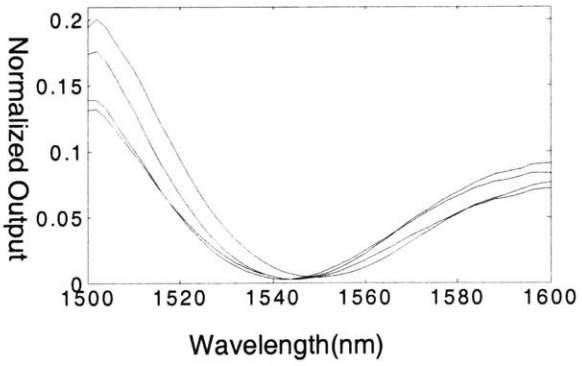

Fig 20 from ref [12]. Improved repeatability measurements for a set of four identical devices with speed2=11.8 mm/s.

The advantage of the feed-foward scheme is that it can successfully control the laser power fluctuations if original fluctuations are within the linear operation of the AOM, which means they are small and have a time scale of a few seconds. The disadvantage is that the AOM adds dispersion and loss to the system, so if the maximum power of the laser is originally 180 mW, it can be difficult to produce favorable devices since there will not be enough power after the AOM for the fabrication of standard waveguides in this study.

4.4 Future work

Because repeatability remains an issue in the study of propagation constant, future work may include further improvement in laser power stability and stage tuning. The spectral period of the Mach-Zehnder interferometer should be set to allow a minimal error in the observation of the change in phase. Change in spectral phase can be observed for larger variations in speed2. This could illuminate when the cutoff for multi-moding occurs and whether there are saturation effects on index or waveguide size as the writing speed is varied. Furthermore, since, the change in propagation constant should be consistent across a straight waveguide, studies can be

performed to confirm whether the spectral shift is linearly dependent upon the length of the waveguide over which speed2 is specified.

An additional experiment which was proposed at the beginning of this study which could be further investigated, is the dependence of propagation constant on writing power. From previous experiments it has been seen that changes in power of 10% can have large effects on waveguide properties. The problem of introducing an additional loss in the beam at a specific position reading using a computer controlled AOM to introduce a change in writing power on the straight portion of the lower arm was difficult to solve using Labview programming. However, as will be discussed further in chapter 5, there may be a method to overcome this limitation using on-board circuitry provided with the stage controller.

The use of femtosecond laser written Mach-Zehnder devices for temperature sensing has already been attempted by at least one group. However, this study was quite qualitative and data was taken by measuring the output intensity of one arm. Preliminary studies on the temperature and mechanical pressure sensitivity of the Mach-Zehnder devices fabricated using the current setup have been performed. With the application of mechanical pressure, there is an observed change in overall intensity output in both ports, however, there is no definitive change in spectral features. This suggests that the current setup for mechanical strain only affects the coupling efficiency of the SMF into and out of the waveguides and not the relative path lengths. To measure the strain sensitivity of the laser-written embedded Mach-Zehnder device, it is necessary to apply a point strain which is precise enough to create a wavelength-scale path length difference between two arms without affecting the input/output coupling ratios or the device characteristics of the couplers. This means the only region of the device which should be affected is the arm, implying the need for mechanical isolation of the other parts of the device. A calculation for the mechanical properties of the substrate is also necessary to determine whether it is practical to apply a mechanical strain of desired strength without creating damage to the substrate.

Preliminary results on the femtosecond laser fabricated Mach-Zehnder device show a clear and significant response to temperature. By attaching a heated resistor, the temperature of both arms

of the MZ interferometer was heated by about 20°C. There is a clear response in the spectral features. However, since the arms of the device are placed close together, it is difficult to create a large temperature difference between them. A calculation of the relative change in arm length using the given thermal properties of EAGLE glass shows that a high amount of spectral phase sensitivity is necessary to detect temperature changes of less than one degree Celsius. Since heating of the glass substrate is usually performed over a period of 10-30 seconds, it would be interesting to quantatively measure the change in the spectral response of the MZ interferometer to characterize the dynamics of thermal diffusion. However, this measurement is limited by the finite data acquisition time of the spectral measurement. A broad-band wavelength source whose output spectra can be recorded in time scales of 1 second can greatly enhance the feasibility of this measurement.

References

[1] N. Pelletier, B. Beche, E. Gaviot, L. Camberlein, N. Grossard, F. Polet, and J. Zyss, "Single-mode ridge optical waveguides on SOG/SU-8 polymer and integrated Mach-Zehnder for designing thermal sensors," *IEEE Sensors Journal* 6(3): 565-70 (2006).

[2] M. Ohkawa, C. Nishiwaki, K. Hasebe, S. Sekine, and T. Sato, "Glass-based integrated optic pressure sensors with a Mach-Zehnder interferometer and with an intermodal interferometer," San Jose, CA, USA, 2000.

[3] K. Okamoto. Fundamentals of Optical Waveguides. Elsevier, Burlington. 2006.

[4] M. Popovic. E. Ippen and F.X. Kartner. "Universally balanced photonic interferometers" Optics Letters. V 31-18. Sep 2006.

[5] K. Minoshima, A. M. Kowalevicz, E. P. Ippen, and J. G. Fujimoto, "Fabrication of coupled mode photonic devices in glass by nonlinear femtosecond laser materials processing," *Optics Express,* vol. 10, 2002

[6] C. Florea and K. A. Winick, "Fabrication and characterization of photonic devices directly written in glass using femtosecond laser pulses," *Journal of Lightwave Technology*, vol. 21, pp. 246-253, 2003.

[7] P. Bado, "Manufacturing of High Quality Integrated Optical Components by Laser Direct-Write," *International Congress on Applications of Lasers and Electrooptics(ICALEO)*, 2003.

[8] P. Yang, J. Guo, and G.R. Burns"Direct-write embedded waveguides and integrated optics in bulk glass by femtosecond laser pulses" *Optics Express.* Vol 44(5). May 2005.

[9] G. Li, K.A. Winick, Ali Said, M. Dungan, and P. Bado, "Waveguide electro-optic modulator in fused silica fabricated by femtosecond laser direct writing and thermal poling" *Optics Letters, 2005*, vol. 31(6), 2006.

[10] C. Mendez, G. A. Torchia, D. Delgado, I. Arias, and L. Roso, "Fabrication and characterization of Mach-Zehnder devices in $LiNbO_3$ writen with femtosecond laser pulses," Mondello, Palermo, Italy, 2005.

[11] Y. Gu. J. Chung, and J.G. Fujimoto. "Femtosecond laser fabrication of directional couplers and Mach-Zehnder interferometers" *Conference on Lasers and Electrooptics(CLEO)*, 2007.

[12] J. Chung, Y.Gu, and J.G. Fujimoto. "Submicron-Period Waveguide Bragg Gratings Direct Written by an 800-nm Femtosecond Oscillator" *Conference on Lasers and Electrooptics(CLEO)*, 2007.

CHAPTER 5: COMBINATION OF LARGE SCALE AND SMALL SCALE SCANNING FOR FABRICATION OF NOVEL STRUCTURES

5.1 Motivation

In chapters 3 and 4 we demonstrate the fabrication of devices by translating the writing sample on a high precision frictionless air-bearing stage. However, due to the relatively large momentum of the stage, there are limitations to the precision and geometry of devices written with this system. To overcome the limitations of structures written with the air-bearing stage, a pair of galvanometer scanning mirrors were incorporated into the system.

One limitation of laser femtosecond waveguide fabrication using the existing setup is the relatively large momentum of the air-bearing stages which limits the precision of small-scale structures. Sudden reversal of direction on the stage results in discontinuities in the waveguide. This can be seen in parts of the fabrication process which require a 90 degree bend. Furthermore, because of the large momentum of the stage, it is difficult to fabricated devices which require large changes in speed. Both of these effects result in limitations on the ability to fabricate more complex devices.

In data presented in chapters 3 and 4, there is a wavelength dependent loss and additional insertion loss resulting from bent waveguide structures. In addition, insertion loss results from a mode mismatch between straight and curved sections of the waveguide. To minimize mode-matching losses between straight and bent waveguides, it is standard practice in lithographic waveguide fabrication to create an off-set or small discontinuity between the waveguides. However, because of the limitations stated above on the air-bearing stage, this kind of structure is difficult to achieve. Creating a waveguide discontinuity requires a sudden acceleration transverse to the direction of motion, and movements which require rapid acceleration cannot be performed in a predictable fashion.

Engineering an additional writing capability which allows for rapid scanning enables the fabrication of novel device structures such as the discontinuities described above. The

combination of large scale and small scale scanning can be an important step toward the developing the capability of writing devices with complex geometries. In particular, the ability to perform rapid scanning of the beam enables the precision control of high-speed writing which is not possible with the air-bearing, stage. This enables the creation of small-scale structures such as discontinuities, microbends and long period grating devices.

Fiber microbend structures and long period grating structures have already been shown to have various applications in sensing. Long period fiber gratings have been demonstrated as indicators for temperature, micro-strain, and changes in the surrounding index of refraction [1]. The long-period grating in a fiber produces coupling between the propagating core mode and co-propagating cladding modes, resulting in a series of attenuation bands in the transmission spectrum. These attenuation bands shift in response to changes in the local environment which affect the period of the LPG, the length of the LPG or the difference between the refractive indices of the guiding and evanescent regions. Traditional LPGs fabricated in standard telecommunications optical fiber have reported temperature sensitivities of 0.03 nm/°C to 0.1 nm/°C [1]. LPGs fabricated in photosensitive B-Ge co-doped optical fibers give enhanced sensitivities of up to 2.75 nm/°C [2]. For refractive index sensing, traditional LPGs have been used to measure a binary solution of xylene in heptane with a resolution in volumetric concentration corresponding to a refractive index change of 6×10^{-5}, comparable to the accuracy of liquid chromatography [3]. Using femtosecond laser irradiation to create optical fiber LPGs, it may be possible to develop embedded devices which have comparable performance. Preliminary measurements on thermal shift of the loss peak in femtosecond written fiber LPGs have been shown to be at around 0.098 nm/°C [4].

The ability to use local scanning to create structures such as microbends can enable the use of femtosecond laser fabricated waveguide devices for microbend sensing applications already demonstrated in conventional microbend devices[5,6]. Fiber microbend grating have a critical period at which there is a peak in transmission. Conventional microbend sensor devices are composed of fibers sandwiched between two plates with periodic grooves. External properties such as displacement, pressure, or temperature that change the distance between these two plates vary the degree of bending, and produce a change in the transmission loss at the critical period.

Although femtosecond laser writing of microbend structures has already been demonstrated [7], the use of a mirror scanning system could improve device quality and adjustability.

To overcome the limitations of the air-bearing stage, we incorporated a pair of 6 mm aperture X-Y galvonometer-based scanning mirrors into the setup (Cambridge Technology model 6215H). See Fig 1 below for a schematic of the layout.

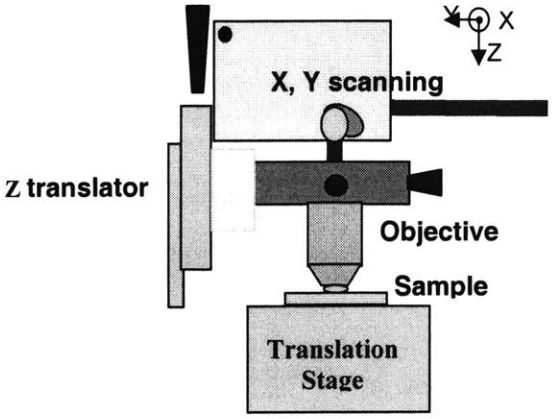

Fig 1. Schematic of combined air-bearing stage and Galvonometer mirror layout.

The mirrors were placed close to the back focal length of the setup and control independently the X and Y directions of beam motion. Labview was used to program the Aerotech air-bearing stage and the scanning mirror motion simultaneously. This allows for the writing of devices which require rapid beam movement and create various small-scale structures with high precision. The Galvanometer mirrors are controlled through analog signals input into a device driver. They posses low noise and high precision within the range of $\pm$ 20 mechanical degrees. Their step response time is 175 μs, scale drift is 50 ppm/ degree C. Their linearity is 99.9% percent and short term repeatability is 8 μrad. The maximum frequency within 5 mechanical degrees of motion is 1.25 kHz and more than 6 kHz within 1 mechanical degree. The roughness of the waveguides is estimated from 8 μrad of position jitter to be 0.03 μm. Because there is a finite aperture on the objective, it is not possible to use the full range of the galvonometer mirror movement, however the maximum travel range achieved on the sample of 30 μm is quite large for small-scale device structuring.

5.2 Development of simultaneous stage and galvanometer mirror control.

One major development which was needed to facilitate the combination of small scale and large scale scanning was the engineering of simultaneous control of the air-bearing stage and galvonometer mirror system. In order to enable fabrication of devices with precise combined global and local structures, the synchronous movement of the air-bearing stage with the Galvanometer mirrors must be controlled to a high degree of accuracy. To this end, a subproject of the galvanometer mirror project involved engineering a computer program which can simultaneously control the stage and output an analog signal to the controller for the Galvanometer mirror. Such a program would be important for application in many other areas which require simultaneous control of the stage and an additional device.

5.2.1 Labview Programming

Traditionally, programming for stage motion is performed in CNC language package which is built in with the simplest graphical user interface, NVIEW MMI, or G code. This is standard machine language, but it does not allow for easy communication with other devices. To facilitate the simultaneous control of stage motion and Galvo mirror motion, the existing programs were migrated into the Labview environment. Using existing Labview subroutines provided by the vendor, we developed a Labview control program which used triggering and execution control to interface with the air-bearing stage as well as the galvonometer mirrors.

In order to produce structures which are a combination of global and local writing, it is necessary to time signals which control the galvanometer mirrors with the motion of the stage such that mirror scanned structures are produced when the beam reaches the desired position in the sample. Shown in Fig 2 is the pseudo code for the position triggering program that was developed in Labview.

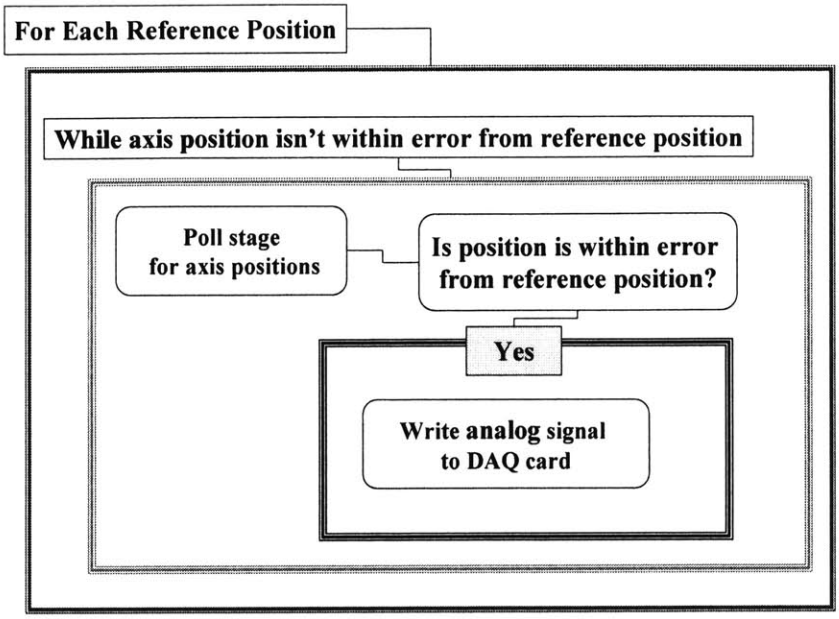

Fig 2. Pseudo code showing position triggering program developed in Labview. The Program polls the axis controller for positions and sends out a signal to the DAQ card when the reference position is reached.

The program is designed to output a periodic signal at certain positions in the writing process. While the program is given a command to run, reference positions are read from a user given filed and a while loop continuously poles the controller for the position of the axis. When the reference position is reached, the while loop is exited and the galvonometer input is sent to the DAQ card. This cycle is repeated for each reference position that is specified. This program demonstrates the important concept of simultaneous controlling both the air bearing stage and a analog voltage controlled device such as a AOM or a set of galvonometer mirrors. However, because of the finite runtime of computer interface with Labview, the position triggering function has very limited accuracy. In position triggering tests with stage movement speed of around 10 mm/s, the error in position trigger was no less than 0.2 mm. This implies that the while loop could only receive a position reference only a few times per second. To understand the limitations of position triggering and how to overcome it, it is important to understand the position feedback mechanisms which govern the stage.

5.2.2 Position Triggering

The controller which interfaces between the CNC program and the stage acts as a dual processor system which coexists with the PC's CPU. The controller is in effect a real-time central

processing unit. It acts as three separate execution units, the library servicer, the CNC engine, and the motion controller. A schematic of the architecture structure of the control system is shown in Fig 3. reprinted from ref [8].

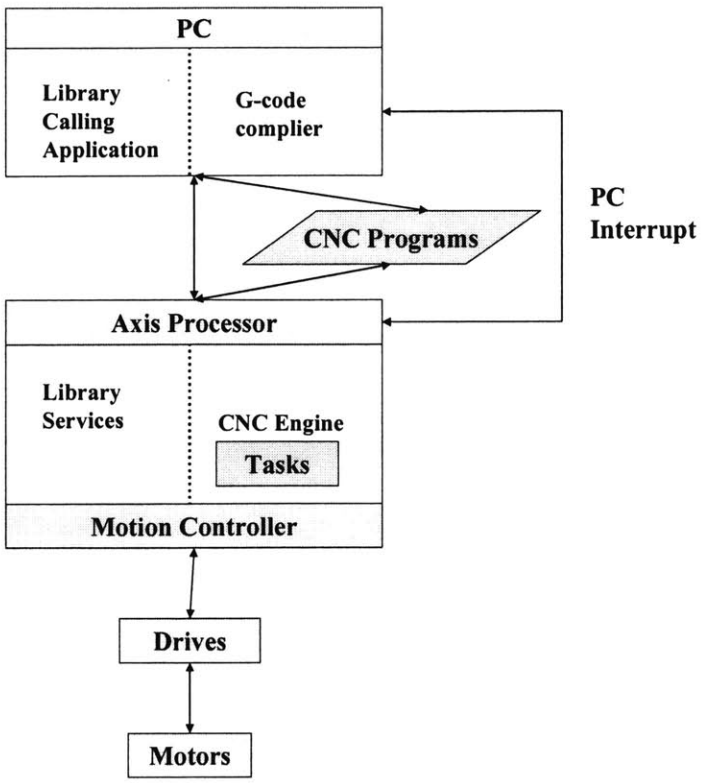

Fig 3 from ref [8] A schematic of the architecture structure of the control system, showing the library servicer, the CNC engine, and motion controller.

The motion controller runs off of an internal interrupt tied to a clock. It executes the servo loop which reads feedback signals and generates velocity and position commands for the device. The stage's position feedback is created by an optical interference signal read from a micron-scale internal marker. There are two sets of markers and the two optical signals have period of 4um and have 90 phase spacing. The encoder processor converts the optical signal into a voltage signal and the motion controller gives position and velocity gains according to user-specified parameters. The servo loop feedback cycle is around 250 kHz. The optical signal which is read by the encoder is expected to have position accuracy of 1 nm.

As discussed in the previous section position trigger through the use of Labview while loops limits position accuracies to 0.2 mm for 10 mm/s motion. The method mentioned above uses a tracking software program external to the motion controller. Because there is a high time cost to testing for both x and y axis at the same time and a slow feedback loop, the position accuracy was severely limited. The execution time of the Labview program delays the trigger signal.

One alternative to avoid errors due to position tracking is time-based triggering. However, this is highly dependent on the knowledge of the stage motion over time, and it can be hard to accurately maintain a reference time base. This method also does not allow for any adjustments during the motion to dynamically correct for fluctuations in velocity which may results in large errors in the triggering position.

The floating stage controller provides a unique high-speed position-based trigger option which is called Position Synchronized Output (PSO) [9]. To improve the cycle time and eliminate other processing problems, this axis-based trigger on the controller is useful. PSO triggers outputs based on the actual axis motions without the effects of external disturbances. The time lag between reaching a position and generating the signal is on the sub-microsecond scale. In addition, PSO enables the triggering of multiple pulses in rapid succession, with trigger rates up to 10 MHz. PSO triggering is directly based on the signal from the encoders for each axis and is therefore time-efficient and accurate. For our application, it may be advantageous to use array-based triggering which fires trigger signals at arbitrary specified positions. See Fig 4 below from ref [9] for the concept of array-based triggering.

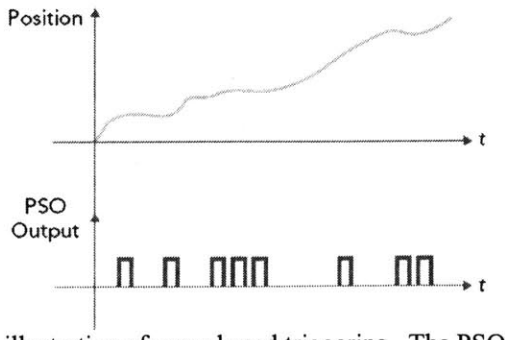

Figure 4 from ref [9] . A illustration of array-based triggering. The PSO sends outputs as the axis reach specified positions which may not be spaced evenly apart. PSO triggering is directly based on the signal from the encoders for each axis and is therefore time-efficient and accurate.

5.3 Galvanometer Mirror Scanned Structures

5.3.1 Basic characteristics

Traditional scanning optical setups involve a 4f system in which two lenses are placed apart by twice the focal length and the beam is scanned from one image plane to another. However, in the current galvanometer setup, due to space constraints, the scanning mirrors are placed close to the back-focal plane of the objective. The maximum optical beam scanning angle for the mirrors is 40 degrees. However, because of the finite aperture size at the back focal plane of the objective, the actual scanning range is limited. The obtainable travel range at the sample was observed by sending a saw-tooth wave to the mirror with amplitude large enough to create cutoff at the edges of the objective lens. As shown in Fig. 5 below, the maximum transverse displacement observed on the sample was around 30 μm. The direction of scanning is right to left. The writing speed is 2 mm/s, and the mirror is scanning transverse to the direction of motion.

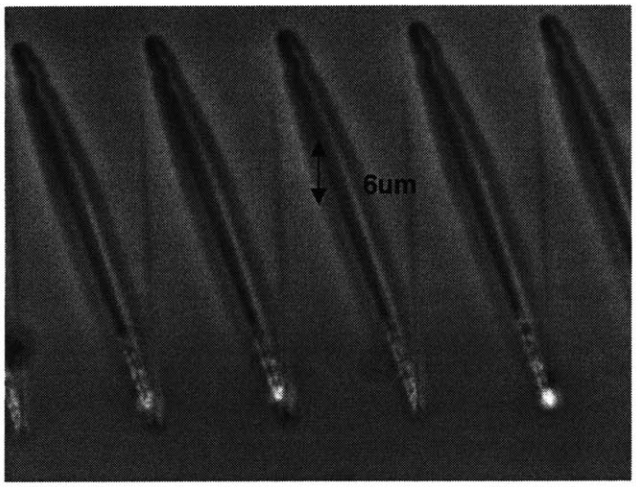

Fig 5. Saw-tooth wave showing cutoff at the edges of the objective aperture. The maximum travel range is 30 μm.

To reduce the roughness of straight waveguides, it is necessary to reduce jitter when a constant voltage is applied to one or both axes of the scanning mirrors to avoid excess loss. This is done by grounding the input whenever a channel is being unused. It is difficult to obtain a quotation for the jitter value of a Galvanometer mirror which is commanded to remain in one position, however, the repeatability value of 8 μrad yields a repeatability of 0.01 μm repeatability at the sample plane. The actual resulting waveguide roughness is expected to be smaller than this value.

5.3.2 Transverse and longitudinal scanning.

To demonstrate the ability to combine local and global femtosecond structuring of integrated, devices, a series of structures were made while scanning the stage x axis in a straight line. Fig 6 below shows the creation of structures by rapidly scanning the beam transverse to the direction of stage motion.

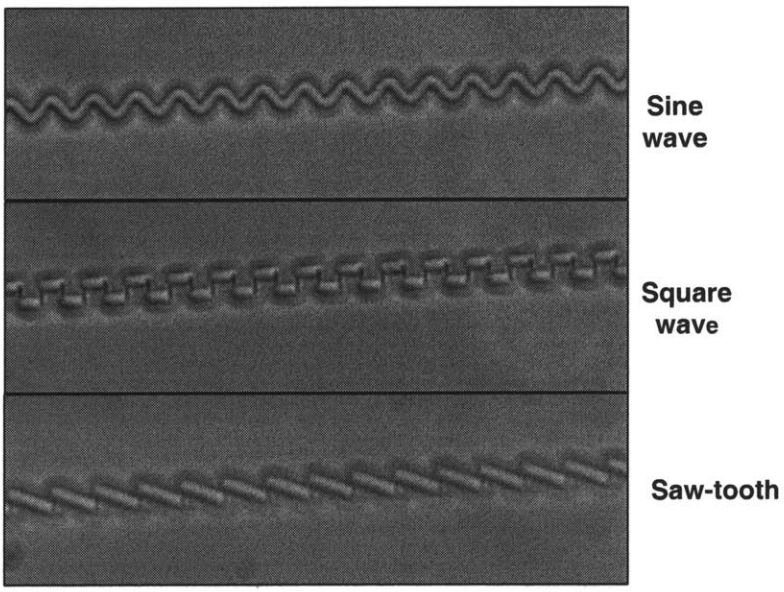

Fig 6. Small scale structures produced by scanning galvanometer mirrors transverse to stage motion. Figures show structures written by sending a sine wave, square wave, and saw-tooth wave to the scanning mirrors.

The three sets of structures were created by sending a sine wave, square wave, and saw-tooth input, respectively, to the galvanometer mirror input. The scanning rate was 200 Hz and stage motion was slowed to 2 mm/s to increase the visibility of the structure. The optical displacement of the beam was 0.24 ° before the objective, resulting in a 4 μm peak-to-peak displacement at the sample. There are effective waveguide discontinuities in both the square wave and saw-tooth wave structures due to the rapid motion of the beam. Also note that singular motions can create waveguides with discontinuities which are not periodic.

In addition to scanning mirrors transverse to the direction of stage motion, it is also possible to scan the mirror which displaces the beam transversely along the direction of motion. This is shown in Fig. 7 below

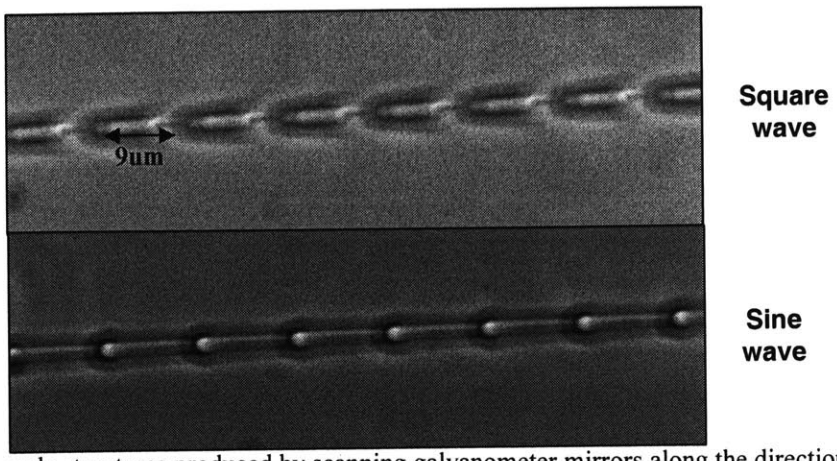

Fig 7. Small scale structures produced by scanning galvanometer mirrors along the direction of stage motion. Figures show structures written by sending a square wave and sine wave to the input of the scanning mirror.

The beam is displaced transverse to the direction of motion by sending a square and sinusoidal wave into the galvanometer mirror input. Notice in this case the resulting structures reflect the change in instantaneous velocity caused by scanning the mirror. The square wave structure, for instance, has nearly constant exposure while the signal is flat and discontinuities where the signal rapidly changes at the edges of the signal. The sine wave signal results in a smooth variation in instantaneous writing speed which is the summation of the mirror scanned motion and the uniform motion. These structures demonstrate the capability of combining stage and galvanometer mirror motion and opens the door for various novel femtosecond written structures. Although periodic structures can clearly be seen, the loss or reflectivity characteristics of the longitudinal structures have not yet been characterized. Further investigation into the waveguide properties of waveguides written with different velocities may open the possibility of creating long-period grating structures using longitudinal scanning. Waveguide writing using transverse scanning enables the creation of structures such as microbends and discontinuities.

References

[1] S. W. James and R. P. Tatam, "Optical fibre long-period grating sensors: Characteristics and application," *Measurement Science and Technology* 14(5): 49-61 (2003).

[2] S. Xuewen, T. Allsop, B. Gwandu, Z. Lin, and I. Bennion, "High-temperature sensitivity of long-period gratings in B-Ge codoped fiber," *IEEE Photonics Technology Letters* 13(8): 818-20 (2001).

[3] T. Allsop, L. Zhang, and I. Bennion, "Detection of organic aromatic compounds in paraffin by a long-period fiber grating optical sensor with optimized sensitivity," *Optics Communications* 191(3-6): 181-90 (2001).

[4] Y. Kondo, K. Nouchi, T. Mitsuyu, M. Watanabe, P. G. Kazansky, and K. Hirao, "Fabrication of long-period fiber gratings by focused irradiation of infrared femtosecond laser pulses," *Optics Letters* 24(10): 646-48 (1999).

[5] N. Lagakos, J. H. Cole, and J. A. Bucaro, "Microbend fiber-optic sensor," Appl. Opt. 26, 2171-2180 (1987).

[6] J. W. Berthold III, "Historical review of microbend fiber-optic sensor," J. Light. Tech. 13, 11931199 (1995).

[7] J. Chung, Y. Gu, and J. G. Fujimoto "Microbend Gratings Fabricated in Glass Substrates via Direct Writing with Near-Infrared Femtosecond Pulses" *Conference on Lasers and Electro-optics.* (2007).

[8] Aerotech. Unidex 600 Series User's Guide.

[9] "PSO Axis based Trigger" www. Aerotech.com.

CHAPTER 6: CONCLUSIONS

The main goals for the study of femtosecond laser fabricated directional couplers were to (a) characterize the spectral behavior for a large range of device parameters (b) show spectral characteristics can be tailored by controlling the physical parameters and (c) design a relatively wavelength-insensitive 3dB directional coupler. After having understood waveguide coupling characteristics and curved waveguide theory, we have demonstrated the fabrication of symmetric directional couplers with interaction lengths varying between 0 and 14 mm. The interaction separation was determined by the size of the waveguide and set at 5 um. We showed that the measurement of these devices over a 100 nm wavelength range yields cross and thru port coupling ratios which agree well with theoretical predictions. Because the coupling ratios vary little for shorter interaction ranges and vary sinusoidally for longer interaction ranges, the spectral behavior can be tailored by controlling the physical parameters of the device. As an example, we showed the design and fabrication of a relatively wavelength-independent 3dB coupler, which was used to build the Mach-Zehnder devices in the next study.

The major goals for the study of femtosecond laser written Mach-Zehnder devices include (a) demonstrating telecom wavelength devices with high contrast ratio and (b) using the spectral characteristics to characterize the propagation constant. We obtained spectral data from Mach-Zehnder devices with different path-length unbalances and shown that their periods vary according to theory. The data demonstrates high contrast ratio although the maxima do not reach unity because normalization with respect to a straight waveguide does not account for other losses such as the wavelength-dependent bending loss. Using the spectral data from different Mach-Zehnder devices, it was possible to calculate a value for the waveguide propagation constant. In addition, we used spectral data from Mach-Zehnder interferometers with a different writing speed in one arm to calculate the change in propagation constant with respect to change in writing speed. Although there are improvements to be made on the repeatability of this measurement, this was the demonstration of an important technique for characterizing waveguide propagation constants as a function of a writing parameter.

Sources of error in both studies include finite stage accuracy and laser power fluctuation. Stage accuracy is usually on the order of nanometers and is a relatively small source of error. To mediate the effects of laser power fluctuation, a computer controlled feed forward power control scheme was implemented using an acousto-optic modulator. In future studies of couplers and Mach-Zehnder devices, it will be important to maintain control over the laser power and take accurate power measurements at the output of the objective lens. This will improve the accuracy and repeatability of all devices.

The third major study described in this thesis is the combination of large scale and small scale beam scanning for the writing of novel devices. A Labview position triggering program was developed to facilitate the simultaneous control of a pair of galvanometer scanning mirrors and the air-bearing stage. We have shown pictures of mirror-scanned microstructures in both the longitudinal and transverse directions relative to waveguide writing. The implementation of this system enables the precise fabrication of devices which contain small scale structures such as long period gratings and microbends.